USE OF A NOVEL MICRO-ELECTRONIC-MACHINING-SYSTEM PRESSURE SENSOR PLATE TO EVALUATE THE MEASUREMENT ERRORS OF A STANDARD TORSIONAL RHEOMETER

by

Wenjie Huang

A thesis submitted to the faculty of
The University of Utah
in partial fulfillment of the requirements for the degree of

Master of Science

Department of Chemical Engineering

The University of Utah

August 2011

The University of Utah Graduate School

STATEMENT OF THESIS APPROVAL

The thesis of **Wenjie Huang**

has been approved by the following supervisory committee members:

Jules J. Magda	, Chair	**5-10-2007** Date Approved
Milind D. Deo	, Member	**5-10-2007** Date Approved
K. Larry DeVries	, Member	**5-10-2007** Date Approved

and by **JoAnn S. Lighty** , Chair of

the Department of **Chemical Engineering**

and by Charles A. Wight, Dean of The Graduate School.

ABSTRACT

The rotational rheometer (cone-and-plate or parallel plates rheometer) is one of the most effective devices for measuring rheological properties of the viscoelastic liquid: the viscosity (η), the first normal stress difference (N_1). However, it has been found practically that some errors were potentially associated with this type of rheometer: The "axial compliance error" is due to the use of linear-variable-displacement-transducer (LVDT) for first normal stress (N_1) measurement, and it is potentially significant in the time-dependent material response measurement. Secondly, the low natural frequencies of sensitive LVDT springs fail in recording the high frequency response of a material. Lastly, misalignment of the sample holder (cone and plate) will change the geometry of the sample. These errors were quantified by performing rheology studies with the LVDT detached and a novel device fabricated with Micro-Electronic-Machining-System (MEMS) technique. The device is a pressure sensor plate of 25mm in diameter. It contains eight miniature capacitive pressure sensors, allowing measurements of the radical pressure profile, from which both the first normal stress (N_1) and the second normal stress (N_2) can be calculated.

The apparent response time of N_1 to start-up of NIST-1490 shear flow was measured. The apparent response time was longer being measured with the LVDT than being measured with the pressure sensor plate, indicating that significant axial compliance er-

rors were present during LVDT measurements. The natural frequency of the LVDT was lower than the high frequency behavior of the tested fluid NIST-1490.

A slight cone-plate misalignment, smaller than the manufacturer's suggested limit, developed a sinusoid-shaped radical pressure profile of the Poly(dimethylsiloxane) (PDMS), corresponding to the axial plane of the tilt. However, this misalignment error can be reduced significantly by averaging the pressure profiles over clockwise and counterclockwise rotation manners.

With the pressure sensor plate, the normal stress ratio, $\Psi = -\frac{N_2}{N_1}$, was measured to be 0.189 for PDMS.

TABLE OF CONTENTS

LIST OF TABLES

LIST OF FIGURES

LIST OF SYMBOLS

η	Viscosity
N_1	The first normal stress difference
N_2	The second normal stress difference
Ψ	Normal stress ratio
Ψ1	The first normal stress difference coefficient
Ψ2	The second normal stress difference coefficient
$\ddot{\Pi}$	Total stress tensor
P	Isotropic thermodynamic pressure
$\ddot{\tau}$	Components of the deviatoric shear stress tensor
$\tau_{\theta\phi}$	Dimensionless deviatioric shear stress
$\tau_{\theta\theta}$	Dimensionless polar normal stress
$\tau_{\phi\phi}$	Dimensionless azimuthal normal stress
V	Velocity
r	Radial position in spherical coordinates
$\dot{\gamma}$	Rate of strain / Shear rate
Ω	Angular velocity of the cone
α	Cone angle
V_ϕ	Main flow velocity

V_θ	Secondary flow velocity
R	Platen radius
M	Measured torque
F	Normal thrust
T	Shear stress
De	Deborah number
F_D	Damping force
W	Separation velocity
C	Damping coefficient
m	Dead weight
x_{max}	The maximum deflection of the normal force spring for a given experimental condition
X	Time-dependent gap between cone and plate
τ	Instrument axial compliance time
λ	Relaxation time
η_0	The zero-shear-rate values of viscosity
f_n	System's natural frequency
ω_n	System's resonant frequency
K	Input signal
ξ	Damping ratio
ω_0	Frequency of the input signals
φ	Phase angle

$\frac{M}{K}$	Signal amplitude ratio
ϕ	Azimuthal angle in spherical coordinates
θ	Perpendicular angle in spherical coordinates
M	Momentum
$\Pi_{22}(r)$	Total stress tensor
g	Gravitational constant ($980 cm/s^2$)
R_g	Measuring limit range of transducer meter
V_f	Full-scale voltage of the transducer meter
V	Measured voltage signal
l	Effective length of the moment arm of the calibrating fixture
K_T	Calibration constant of torsion bar
K_N	Spring constant
ω_i	Dimensionless shear rate / Weissenberg number

LIST OF ABBREVIATIONS

AC	Alternating current
CP	Cone-and-plate rheometer
DC	Direct current
FRT	Force rebalance transducer
LVDT	Linear variable displacement transducer
MEMS	Micro-electrical-machining system
NIST	National Institute of standards and testing
NSS	Normal Stress Sensor
PDMS	Polydimethylsilane
PP	Parallel-plates rheometer
SOI	silicon-on-insulator
SRM	Standard reference material
WRG	Weissenberg rheogoniometer

ACKNOWLEDGMENTS

In this thesis work, there are many individuals to be acknowledged for their help. First of all, I wish to express sincere appreciation onto my adviser, Professor J. J. Magda's for his assistance, guidance, encouragement, and support throughout my study and research, which improved my professional skills. Grateful appreciation is extended to Professor Milind D. Deo and K. Larry DeVries, members of my supervisory committee, for their valuable time and encouragement. Special appreciation is also expressed to Rheosense, INC. (San Ramon, CA) and Doctor S.G. Baek, CEO of Rheosense, INC., for supplying their newly made NSS and financial support. I also appreciate Professor Greg McKenna and Doctor S. X. Fu in Texas Tech University for allowing and training me to use their ARES rheometer. The financial support of this study is from grant NAG8-1665.

Finally, I am grateful to my husband, Sheng Cao, my daughter, Cynthia Cao, my parents, and my sister for their great support and love.

CHAPTER 1

INTRODUCTION: RELEVANCE AND SCOPE

Polymers are a large class of materials consisting of many small molecules or monomers that can be linked together and form long trains. They are known as macromolecules. Humans have been taking advantage of the versatility of polymers for centuries. Natural and synthetic polymers can be produced with a wide range of stiffness, strength, heat resistance, density and price [1]. With continuous research into the science and applications of polymers, they are playing an ever increasing role in society.

The processing behavior of molten thermoplastics depends on their rheological properties, which are often measured in cone-and-plate rheometers where shear flow is produced [2]. There are three rheological properties in the shear flow field (see Chapter 2 for definitions): the viscosity η, the first normal stress difference N_1 and the second normal stress difference N_2. The cone-and-plate rheometer is one of the most common types of commercial rheometers in the world. However, the cone-and-plate rheometer will not give the correct values for the three properties if the flow field is disturbed by a slight misalignment of the cone and the plate. Other measurement errors associated with the rheometer transducer, such as compliance error and response time error, can also distort the results. Unfortunately, most rheologists have not developed a method to check the magnitude of these errors. In our lab, we use a novel pressure sensor plate recently

available to detect all the errors mentioned above. Details of this pressure sensor plate and associated method are presented in Chapter 2 and 3. The principle goal of this thesis work was to use this novel pressure sensor plate to evaluate potential measurement errors of a standard cone-and-plate rheometer.

During polymer processing, unfavorable flow instabilities may be caused by the elastic properties of materials [3-9]. Theoretically, elastic instabilities are often directly associated with the ratio of the second and the first normal stress differences, $\psi = -\frac{N_2}{N_1}$, which is called the normal stress ratio. For certain type of polymer processing operations, e.g., coextrusion and wire coating, the magnitude of ψ can be used to predict whether the polymer melts operation is stable or not [10-12]. Consequently, accurate measurement of first and second normal stress differences is very important regarding industrial polymer processing. In this sense, the second goal of this thesis work was to use the novel pressure sensor plate to measure an accurate value of ψ for the polymer fluids tested.

This novel pressure sensor plate, called the "Normal Stress Sensor (NSS)" was obtained from Rheosense Inc. (San Ramon, CA) and is based on Micro-Electrical-Machining System (MEMS) technology. This thesis is mainly about the practical application of the NSS to obtain the radical pressure distribution in order to explore measuring system errors, misalignment error, compliance error and transducer response time error and to measure the normal stress differences simultaneously. Poly(dimethylsiloxane) (PDMS) was used as a test polymer melt to compare the frequency response due to the different natural frequencies of the conventional normal force transducer, i.e., linear variable differential transducer, and the NSS. The first and

second normal stress differences of PDMS were also evaluated with the help of the pressure sensor plate. Measurements of the apparent response time of N_1 to start up of flow shear flow were carried out with and without the working Linear Variable Displacement Transducer (LVDT) to study the effect of the axial compliance due to the finite stiffness of the LVDT transducer system. The apparent response time of N_1 was determined directly *via* the duration of the starting-up behavior and was compared with the theoretical value predicted by the equation derived from Hanson *et al.* [13]. In this experiment, a standard NIST (National Institute of Standards and Testing, Gaithersburg, MD) viscoelastic fluid SRM (Standard reference material) 1490 was used.

The definitions of the three shear flow properties of materials will be presented in the next section. Possible system errors will be discussed in Section 2.3 after the cone-and-plate measuring system is introduced.

CHAPTER 2

BACKGROUND AND LITERATURE SURVEY

2.1 Importance of the Normal Stress Differences, N_1 and N_2

Flow instabilities [2-7] occur in the processing of polymer melts and polymer solutions under certain flowing conditions. **Figure 2.1** shows the stable and unstable flows of the viscoelastic fluid when it was processed in an extruder [6], which is a very popular industrial polymer processing method. If the flow instability is developed in an industrial polymer processing, it will lead to product defects like surface roughness, which is called "shark skin" in industry [2-4], or the interfacial irregularity (**Figure 2.2**) in a multiphase coextrusion [7].

Numerous methods [8-12] have been developed to predict the velocity field of different type processing flows in order to avoid the flow instabilities. It is known that this unfavorable flow instability is often caused by the elastic properties of materials. Theoretically, elastic instabilities are linked with the values of the normal stress ratio $\psi = -\frac{N_2}{N_1}$ [8-10]. In general, the relationship of the fluid instabilities and the rheological properties, i.e. the first and the second normal stress differences (N_1, N_2) or coefficients (ψ_1, ψ_2) can be predicted by following model: large values of the first normal stress difference coefficient ψ_1 tend to destabilize curvilinear shear flows of elastic liquids, leading to flow instabilities at low shear rates; on the contrary, large negative values of

the second normal stress difference coefficient ψ_2 tend to stabilize curvilinear shear flows. Therefore, unstable flow behavior can be expected for polymer melts in flow fields with curved streamlines when the value of the normal stress ratio $\psi = -\frac{N_2}{N_1}$ is small in magnitude [14]. However, for coextrusion of two different immiscible polymer melts through a noncircular die (**Figure 2.2**), unstable behavior is known to occur when N_2 has large negative values [7,14]. Based on this theory, measurement of the first and second normal stress differences becomes significantly important regarding the industrial polymer process. Unfortunately, many constitutive equations or the stress-strain relations, which are essential to the validity of the numerical results, are uncertain for commercial polymer melts. Numerical technique can be applied to a limited field to simulate some elastic fluids like Boger fluid [15] or dilute polymer solutions [16], which are simpler and better understood in terms of the constitutive equations.

Simultaneously, experimental techniques have been used to obtain the three rheological properties, i.e., the viscosity and the two normal stress differences, not only for simple elastic fluids but also some very important commercial polymer melts, such as polyethylene, polystyrene, etc. [7,17]. However, some experimental methods are controversial because of their theoretically uncertainty [18]. Some other methods are widely accepted in theory, but due to the mechanical and operation difficulties [19,20], they may not be accurate. This is especially true for measurements of the second normal stress, which is much smaller than the other two properties for the normal shear-thinning polymer melts. The cone-and-plate pressure distribution method, which has long investigated and developed in our lab [14,21-26], is among these methods. But, due to the

research work of many rheologists in several decades (from 1964 to present), this method has become more and more accurate and reliable. The details introduction of this method will be reviewed in the latter sections in this chapter.

2.2 Ideal Cone-plate Rheometry for Simple Shear Flow

The state of stress for a non-Newtonian fluid in any arbitrary flow field can be described by a second order tensor; the total stress tensor $\ddot{\Pi}$ is given as [27]:

$$\ddot{\Pi} = \ddot{\tau} - P\ddot{\delta} = \begin{pmatrix} \tau_{11} - P & \tau_{12} & \tau_{13} \\ \tau_{21} & \tau_{22} - P & \tau_{23} \\ \tau_{31} & \tau_{32} & \tau_{33} - P \end{pmatrix} \quad (2.1)$$

In this equation, P is the isotropic thermodynamic pressure; $\ddot{\tau}$ are components of the deviatoric shear stress tensor, and subscripts 1, 2, and 3 denote the three coordinate directions. This notation for subscripts will be used throughout this thesis. Components on the diagonal of the total stress tensor are called *normal stresses*, and the off-diagonal components are called *shear stresses*. For an isotropic fluid, the stress tensor is usually assumed to be symmetrical, that is, $\ddot{\Pi}_{ij}$ equals to $\ddot{\Pi}_{ji}$. Thus, there are six independent stress components in the symmetrical total stress tensor. In real flows, flow kinetics are so complicated that all six components of $\ddot{\Pi}$ should be assumed to be nonzero. Experimentally, it is very difficult to measure all six stress components. Therefore, we require a reduction in the number of stress components in order to measure properties.

Such a reduction can be accomplished by imposing a steady shear flow like planar couette flow (**Figure 2.3**). In a simple shear flow, the velocity field is given by:

$$V_1 = V(y), \text{ and } V_2 = V_3 = 0 \tag{2. 2}$$

For this type of flow, the rate of strain tensor is given as

$$\ddot{A} = \begin{pmatrix} 0 & \dot{\gamma} & 0 \\ \dot{\gamma} & 0 & 0 \\ 0 & 0 & 0 \end{pmatrix}, \qquad \text{where } \dot{\gamma} = \frac{dV_1}{dy} \tag{2. 3}$$

in this relation, $\dot{\gamma}$ is defined as rate of strain, or a normal definition shear rate. The shear rate in a steady shear flow will not change due to the coordinate transformation $x' = -x$, $y' = -y$, and $z' = -z$, due to the flow symmetry. Thus the total stress tensor, a function of the shear rate, has the following nonzero stress components:

$$\ddot{\Pi} = \begin{pmatrix} \tau_{11} - P & \tau_{12} & 0 \\ \tau_{21} & \tau_{22} - P & 0 \\ 0 & 0 & \tau_{33} - P \end{pmatrix} \tag{2. 4}$$

This equation is valid only if the total stress tensor is symmetric. So the three material functions for simple shear flow are defined as:

shear stress $\tau_{12} = \tau_{21} = \eta\dot{\gamma}$,

the first normal stress difference $N_1 = \tau_{11} - \tau_{22}$ or

the first normal stress difference coefficient $\psi_1 = \frac{N_1}{\dot{\gamma}^2}$,

the second normal stress difference $N_2 = \tau_{22} - \tau_{33}$ or

the second normal stress difference coefficient $\psi_2 = \frac{N_2}{\dot{\gamma}^2}$.

For the time being, the other definition is usually considered:

the normal stress ratio $\psi = -\frac{N_2}{N_1} = --\frac{\psi_2}{\psi_1}$.

The definition of the first and second normal stress differences (N_1 and N_2) by subtraction of two normal stresses cancels out the thermodynamic pressure, which can not be independently measurable from the deviatory normal stresses. The steady shear flow can also be categorized as one of the many types of viscometric flows for which the rate of strain tensor is equivalent to Equation 2.3 on a local level. As a matter of fact, steady shear flow in the ideal cone-and-plate is another type of viscometric flow. In the ideal cone-and-plate rheometer, $\dot{\gamma}$ has the same value at all locations within the gap and is given by $\dot{\gamma} = \frac{\Omega \cdot r}{\cos(\alpha) \cdot r} = \frac{\Omega}{\cos(\alpha)}$, where Ω is the angular velocity of rotation and α is the cone angle. As discussed in Section 2.3, misalignment will lead to a violation of the uniform shear rate assumption.

2.3 The Traditional Measuring System for the First Normal Stress Difference

A linear variable differential transducer (LVDT) is presently applied in the most traditional rotating cone-and-plate rheometers (Weissenberg Rheometer) in our lab. The detailed schematic diagram of the LVDT-cone-and-plate rheometer is shown in **Figure 2.4**. The tested sample is held between the cone and plate. During measurement, the normal thrust from the static top plate is transmitted along air bearing torsion bar (barely no friction) to a cantilever spring. When the cone is rotating, correspondent stresses occur throughout the simply sheared sample inside the cone and plate and response in three directions: the shear stress in the flow direction, the first normal stress difference in the

normal direction and the second normal stress difference in the neutral direction. For an ideal cone-and-plate rheometer, the flow field is viscometric with uniform shear rate and given by:

$$V_\phi = r\Omega \cdot \frac{\frac{\pi}{2} - \alpha}{\frac{\pi}{2} - \theta}, \text{ and } V_r = V_\theta = 0 \tag{2. 5}$$

where r is radial position in spherical coordinates; Ω is the angular velocity of the cone; α is the cone angle.

The shear stress and the first normal stress differences are related to the measured toque M and axial normal thrust F [28]:

$$\tau_{r\phi}(\gamma, t) = \frac{3M(\gamma, t)}{2\pi R^3}, \tag{2. 6a}$$

$$N_\theta(\gamma, t) = \frac{2F(\gamma, t)}{\pi R^2} \tag{2. 6b}$$

From Equation 2.6b, the first normal stress difference can be determined by measuring the total vertical thrust F on the plate using the deflection of LVDT. As the vertical thrust deflects the spring from its null position, the LVDT generates an electronic signal (in volts) with intensity proportional to the deflection at the free end of the cantilever spring. This voltage value is directly proportional to the thrust developed by the test fluid.

An LVDT (**Figure 2.6**) is one type of displacement transducer with a high degree of robustness. In the Weissenberg Rheometer, LVDT is very sensitive for measuring the

normal thrust. According to the tests in our lab, the smallest pressure that could be reliably measured by the LVDT in Wessenberg Rheometer is around 15 Pascal [25]. However, the LVDT works due to the displacement, which changes the position of the top plate in the Rheometer, causing the *instrument compliance*. This leads to a violation of Equation 2.5, which is based on the assumption that the geometric tip of the truncated cone just touches the surface of the rheometer plate. Details of how the compliance of the LVDT spring changes the sample gap will be discussed in the following section.

2.4 Potential Errors in the Use of the Cone-and-plate Rheometer

2.4.1 Misalignment of the Cone-and-plate Rheometer

Equations 2.5 and 2.6 are based on the assumption that the flow field is viscometric with uniform shear rate $\dot{\gamma}$ throughout the cone-and-plate gap. This is not true if the cone and plate are misaligned. There are three types of misalignment as demonstrated in **Figure 2.7**: (1). cone and plate are not concentric (**Figure 2.7 (a)**); (2). axis of stationary plate is not perpendicular to the vertical rotation axis ---- the stationary plate is tilted (**Figure 2.7 (b)**); (3). axis of rotation is not perpendicular to the vertical axis of the stationary plate ---- the rotating cone is tilted (**Figure 2.7 (c)**).

The misalignment of concentricity and flatness of the cone-and-plate Rheometers, including the Weissenberg Rheometer in our lab, are unavoidable but could be minimized. A dial gauge is used for the adjustment. According to the manual of Weissenberg Rheometer, a minor misalighment smaller than 12.7 microns (0.0005 inch) reading in dial gauge for the concentricity, and maximum 2.5 microns or 0.0001 inch reading in dial gauge for the flatness were negligible misalignment errors. However,

these criteria have not been justified; and only sparse research work has been reported studying considerable misalignment errors beyond the negligible limit [29].

One of these misalignments, i.e. tilted cone with respect to the vertical axis of the stationary plate, is the only type of misalignment that has been studied and reported by rheologists (Greensmith *et al.*, Taylor *et al.*, Adams and Lodge, Dudgeon and Wedwood) [30-33]. The phenomenon was first observed by Greensmith *et al.* (1953) [30]. Taylor *et al.* (1957) [31] investigated it experimentally and theoretically. These two research groups both used Newtonian incompressible fluid in parallel plate geometry. For a Newtonian liquid, the pressure is expected to be atmospheric at all locations within the rheometer in the absence of inertia. They found the 'wedge effect', also called 'Michelle bearing effect'. The wedge effect means that the tilted misalignment results in non-parallelism of the two plates and cause a converging flow in one half of the gap and a diverging flow in the other half, the two halves being separated by the vertical plane perpendicular to the line of greatest slope of the nonhorizontal plate. When the gap is narrow and the liquid is viscous, a very small degree of nonparallelism can lead to a large pressure maximum in the converging flow and a large pressure minimum in the converging flow. In addition, they also found that the pressure distributions over the two halves of either plate were symmetrical apart from the difference of sign so that the wedge effect could be eliminated, at least for Newtonian fluid, by averaging the pressures measured with two senses of rotation: forward and reverse. Adams *et al*. (1963) [32] continued the previous studies, and extended the investigation into cone-and-plate geometry, still employing Newtonian liquids. The pressure distribution measured using pressure manometer in both geometries, parallel-plates and cone-and-plate, were now

known to be inaccurate due to the "hole pressure error" (**Figure 2.8**) [34]. **Figure 2.9** shows the qualitative shape of the radial pressure profile measured by Adams and Lodge for a Newtonian fluid in a tilted cone-and-plate rheometer. As shown in the diagram, the local pressures were measured along a line perpendicular to the greatest slope of cone tilt. The measured pressure profile displays the symmetrically disposed maximum and minimum interchange on reversal of the rotation sense in direction. The average of pressures recorded at the same position on the plate for the two rotating directions was close to zero (dashed line in **Figure 2.9**). These results were in agreement with Saffman and Taylor's (1963) that zero pressure points are along the line with the greatest slope; the distribution of pressure along the line of greatest slope displayed a small but definite nonuniformity, which was independent of the rotation direction. Even with the same conditions like same rotation speed and rim separation, this phenomenon differed with respect to the variable types of geometry, i.e., parallel plates vs. cone-and-plate. For example, the greatest pressure occurs near the axis of rotation and is larger in the cone-and-plate system than that in the parallel plates system [32]. It is worthwhile to notice that the unit of pressure was not marked in **Figure 2.9** to emphasize the pressure outline in the flow field. As a matter of fact, the pressure was small, which would make the result questionable. Dudgeon and Wedgewood (1993) theoretically simulated the flow fields of various Non-Newtonian elastic fluids in the slightly misaligned cone-and-plate rheometer [33]. Their results show: (1). For Newtonian flow, the polar normal stresses were symmetric but change in sign on the line at right angle to the line of the greatest slope in cone tilt, which was in agreement with earlier pressure profile results for Newtonian fluids in tilted cone-and-plate flows. (2). For non-Newtonian flow, the polar normal

stresses profile became asymmetric with regard tilt axis line; higher elasticity of the fluid is, higher asetricity of the polar normal stresses were expected (**Figure 2. 10**).

Dudgeon and Wedgewood theoretically predicted the different misalignment effects on fluid with various viscoelasticity properties. Their results await experimental verifications. The difficulty of verifying their results lies in the facts that no instruments are able to measure the stresses tensors directly. In this thesis, the noval Micro-Electro-Machining-System (MEMS) pressure sensor plate was used and it solved the technique difficulty. This MEMS plate can accurately measure the local pressure distribution of the fluid so that the fluid disturbance due to a negletible misalignment (on the dial gauge) could be observed directly. Consequently, former studies on the misalignment were confirmed. Also a fluid irregularity, the wobble error, was detected for the first time in this thesis research. And the most important achievement of this thesis work is a detailed study of how the tilt-axis misalignments that cause a nonuniform shear distort the radical pressure distribution.

This thesis research differs in various ways with the previous studies: firstly, it focused on cone-and-plate rheometry; secondly, it focused on the unavoidable small misalignment; thirdly, it employs a novel pressure sensor plate experimentally with non-Newtonian fluids. Presently, no literature was reported on the study of the other type of misalignment, i.e., the tilted stationary plate with respect to the vertical axis of rotation. The effects of the third type of misalignment remain unknown presently.

2.4.2 Axial Transducer Compliance Error of the Cone-and-plate Rheometer

This section reviews one of the main equipment defects, instrument compliance. Instrument compliance contributes to the inaccuracy of N_1 measurements in the traditional rotational rheometers. A precise transient normal force measurement in the rotational rheometers requests unchanged gap geometry because a variation of the gap, gap opening, will cause undesirable sample flow in the radial direction. With the presence of the radial flow, the apparent time-dependent normal stress behavior will not correspond to a true material property, but the instrument parameters. Such a "gap opening" effect is defined as instrument compliance. Instrument compliance, unless properly taken into account, may introduce considerable errors into dynamic rheological measurements [35-38]. In traditional rotational rheometer measurements, instrument compliance will introduce errors in two ways: (1), change in the original rotation position in shear stress transducer; (2), change in the previously set separation of the cone and the plate, which can also be called *compressive/axial compliance error*. This thesis work focused on the effects of axial compliance in the measurement of N_1.

The compliance error arises due to the mobility of the top plate/cone connected to armature of the LVDT via a spring (**Figure 2. 11**). As the test fluid is sheared, a normal thrust is generated due to the first normal stress difference, which pushes the top plate/cone upward, thus changing the deflection of the measuring spring and the position of the top plate/cone and subsequently the gap between the cone and plate. This process is sketched in **Figure 2.11**. Details of the transducer LVDT, which are essential to understand the measuring system, are discussed in Chapter 3. According to fluid

mechanics analysis of the cone-and-plate rheometry, accurate gap setting of the truncated cone and plate is crucial to the accuracy of the measurements. The departure of the gap from its correct value introduces both a steady-state and a transient error:

1. Steady-state error: the hypothetical tip of the truncated cone will not just touch the top surface of the rheometer plate, as required to obtain the correct steady-state velocity field within the sample (Equation 2.5).

2. Transient measurement error: even if the steady-state axial compliance error is small, it will be impossible to measure the true material response time. The time it takes the gap to change (the "instrument time") is comparable to the material response time [13,35-36].

Practically, one can adopt springs that are stiff enough to make the compressive compliance error small enough to be neglected. Additionally, the stiff transducer will also reduce the response time of the transducer, thus reducing the instrument response time. On the other hand, spring with too large constants will fail in detecting a relatively small N_1 value, resulting in low sensitiveity. One can eliminate by readjusting the rheometer gap once steady flow is observed, which is the working principle of the force rebalance transducer (FRT) from TA Instruments, Inc. [37]. However, the transient measurement error cannot be eliminated unless one dispensed with the LVDT uses and uses an alternative measuring method, such as the pressure sensor plate used in this thesis work. Further more, the FRT uses an active servo loop to control the rheometer gap that may result in thermal expansion of the sample during prolonged test (**Figure 2.12**) [37].

The existence of the instrument compliance and its influence on dynamic rheological measurements has been explored previously and the physical definition of

instrument complicance in terms of response time of either the instrument or the material was developed [13,38-42].

Stretton's test (**Figure 2.13)** successfully demonstrates the instrument compliance in traditional thrometers. The constant C in **Figure 2.13** corresponds to a dashpot parameter created by sandwiching the test fluid between cone and plate, K represents the normal force cantilever spring constant and m is the dead weight. With the inertia term, damping term, normal force spring term and the force function taken into account, the equation of motion based on Stratton's test can be given as [35]:

$$\bar{F}h(t) = m\frac{d^2(x(t))}{dt^2} + C\frac{d(x(t))}{dt} + Kx(t) \tag{2. 7}$$

Among these terms, the dependence of the damping coefficient on the geometrical variables of the instrument and on the rheological properties of the test fluids was considered. The damping force, F_D, corresponding to an infinitesimal change in separation between the cone and the plate, with incompressible Newtonian fluid inside, was expressed as [35]:

$$F_D = -\frac{6\pi\eta R}{\alpha^3}W \tag{2. 8}$$

where W is the separation velocity. The damping force corresponding to the compliance force in the cone-and-plate fluid is directly proportional to the viscosity, η, and the plate radius, R, but inversely proportional to the third power of the cone angle, α^3. In another word, a small cone and plate radius or the relatively large angle of the gap of the cone and the plate will help to reduce the compliance error [35]. It should be noted that the

separation of the cone and plate is considered infinitesimally ralative to the cone and plate radius because the inertia term in Equation 2.7 was neglected. On substituting the damping coefficient from Equation 2.8 into Equation 2.7, the solution for the time dependent rheometer gap becomes [35]:

$$X = \frac{x}{x_{\max}} = 1 - e^{-t/\tau} \quad , \tag{2. 9}$$

And [9, 39]

$$\tau = \frac{6\pi\eta R}{K\alpha^3} , \tag{2. 10}$$

where $x_{\max}$ is the maximum deflection of the normal force spring for a given experimental condition. The system response time, τ , in Equation 2.10 is important and used as a guide to determine conditions under which the rheometer can reliably measure the normal stress growth.

Meissner *et al.* (1972) [38] firstly added a closed loop feedback system to a classic Weinssenberg rheogoniometer (WRG) with a sufficiently stiff spring and minimized the compliance error in the normal force measuring system. They found out that the measured onset response of melted polymer was often a combination of material and apparatus responses. Hansen *et al.* (1975) [13] quantitatively determined the relationship of the characteristic response time, τ , of the normal force measurement and the characteristic time of the test fluid (material): the time for the apparent normal stress to reach 63.2% of shear flow steady state should be much greater than the value of τ theoretically deduced for a given apparatus configuration and fluid viscosity. In such a

way, the value of τ for the normal force measuring system was deduced theoretically. However, Hansen's result was based on Equation 2.10, which assume a Newtonian sample and under the condition of neglecting inertial fluid term in Equation 2.7. It was doubtful whether Hansen's work was feasible for non-Newtonian flow. *Zapas et al.* (1989) [35] developed a more universal relationship to describe the dramatic impact of compliance error of constrained geometry regarding to the response time in uniaxial extension and compression response, which was in agreement with single-step stress relaxation of BKZ-type fluid, to the nonlinear region. All these studies contributed to a complete description of the compliance phenomenon in various aspects such as compliance time, instrumental accuracy, axial displacement, and so on.

In this thesis, Hansen's criterion will apply to test the effectiveness of classic Weinssenberg rheogoniometer (WRG) without FRT system in measuring the transient N_1 for two test fluids (non-Newtonian fluid), in terms of instrument axial compliance time, τ . In order to measure the longest relaxation time λ of the sample being tested, instrument axial compliance time, τ , should be much less than λ. The relaxation time λ can be independently estimated with the experimentally accessible material properties, i.e. the zero-shear-rate values of viscosity and first normal stress difference coefficient, η_0 and $\Psi_{1,0} = \frac{N_{1,0}}{\dot{\gamma}^2}$, by the relationship of $\lambda = \frac{\Psi_{1,0}}{2 \cdot \eta}$ [9,13]. In the absence of a significant instrument axial compliance time, λ should also approximately equal to the time it takes N_1 to reach 63.2% of its steady state value after onset of shear flow.

2.4.3 Effects of Natural Frequency on the Measuring System:

Transducer Response Time

Physically, a system tends to oscillate at maximum amplitude at a certain frequency. This phenomenon is called resonance, and this frequency is known as the system's resonant frequency, f_n. When damping is small, the resonant frequency is approximately equal to the natural frequency of the system, which is the frequency of free vibrations. Commonly, natural frequency is related to resonant frequency by:

$$f_n = \frac{\omega_n}{2\pi} = \frac{1}{2\pi}\sqrt{\frac{k}{m}} \tag{2. 11}$$

The dynamic operation of many measuring systems can be adequately represented by a second order differential equation. For instance, the elementary galvanometer exhibits second-order behavior is expressed by a single differential equation [43]:

$$\frac{d^2S}{dt^2} + (2\xi\omega_n)\frac{dS}{dt} + (\omega_n{}^2)S = (\omega_n{}^2 K)V \tag{2. 12}$$

Equation 2.12 relates the input signal V (volt) to its output signal S (light-beam displacement). Equation 2.12 includes three important instrument constants of a galvanometer: K, the sensitivity of the instrument in $\left[{}^{in}/_{V}\right]$; $\omega_n = \sqrt{\frac{k}{m}}$, the natural circular frequency of the instrument in $\left[{}^{rad}/_{\sec}\right]$, or the natural frequency in cps; and ξ, the damping ratio. The second order system frequency response can be demonstrated by Equation 2.13:

$$\frac{M}{K} = \frac{{\omega_n}^2}{\sqrt{\left({\omega_n}^2 - {\omega_i}^2\right)^2 + \left(2\xi\omega_n\omega_i\right)^2}} \qquad (2.\ 13)$$

This equation demonstrated the importance of the damping ratio and the natural circular frequency. The curves in **Figure 2.14** are based on equation 2. 13 and demonstrate the frequency response, ω, of the typical second-order instrument:

(1), for very low input-signal frequencies $\left(\omega_i << \omega_n\right)$, the instrument responses ideally;

(2), for very high input-signal frequencies $\left(\omega_i >> \omega_n\right)$, the instrument is completely incapable of "following" the input signal; (3), the frequency response is the instrument behavior when the input signal frequency ω_i happens to be nearly the same as the natural circular frequency ω_n.

The compliance error of the measuring system of the Weinssenberg rheogoniometer displays a typical second-order response (Equation 2.7). Consequently, the natural circular frequency, ω_n, of the LVDT measuring system is critical because the system cannot measure the true frequency response of the material at frequencies greater than ω_n . The Weinssenberg rheogoniometer bears LVDT spring with a moderate stiffness in order to maintain a fairly high sensitivity for steady-state measurements. On the other hand, the natural frequency of noval pressure sensor plate is much higher: $f_n \cong 137kHz$ [44]. So a goal of this thesis was set to compare the apparent frequency response of a sample measured with the LVDT and the pressure sensor plate.

2.5 Experimental Techniques for Measuring the Second Normal Stress Difference

The stresses in a simple shear flow can be fully characterized by three independent functions: viscosity (η), the first and second normal stress differences (N_1, N_2) and the first and second normal stress difference coefficients (ψ_1, ψ_2). Here the normal stress differences are relative to the normal stress difference coefficients as [45]:

$$N_1 = \psi_1 \dot{\gamma}^2 \ , \ N_2 = \psi_2 \dot{\gamma}^2 \tag{2. 18}$$

where $\dot{\gamma}$ is the shear rate in the shear flow. The second normal stress difference coefficient ψ_2 is much smaller compared to the first normal stress difference N_1 in magnitude and was assumed to be zero by Wessenberg (the 'Wessenberg hypotheses'). In 1970's, it was found that the second normal stress might play an important role on rheological fluid instabilities. Consequently, compared to the fully developed commercial rheometers for measuring η and ψ_1, the techniques for measuring ψ_2 are limited and have not been developed for commercial use. Devices were customized for scientific measurements. Early measurements by Lodge *et al.* (1975) confirmed the presence of N_2, while their results were distorted to be positive by the "hole pressure error" [34]. Ginn and Metzner (1969) **[**46**]** compared total thrust measurements in cone-and-plate and plate-and-plate rheometers and found that N_2 should be negative values. The measured normal stress coefficients, $\psi = -\frac{N_2}{N_1}$, were very small (**Table 2.1**) [23,26-27,44,46-70].

Table 2.1 also shows a summary of the methods applied to determine the normal stress coefficient ψ .

The early results of the normal stress ratio ψ were mostly small to zero or sometimes even negative and were inconsistent, indicating that some methods were not appropriate. There has been a steady improvement in methods for measuring ψ from the radical pressure distribution in cone-and-plate rheometry (methods 14, 16, 17 in **Table 2.1**). Among all the methods (**Table 2.1)**, measuring pressure distribution in the fluid field using a novel "MEMS" pressure sensor plate is one of the most accurate methods [21-25]. MEMS, which stands for Micro-Electric-Machining-Systems, is a semi conductor processing technique. This technique makes it possible to fabricate miniature pressure sensors with areas less than 1 mm^2, thus allowing considerable decrease in the size of rheometer plate. The technical details of the pressure sensor plate will be presented in Chapter 3 when the experimental implementation is explained.

2.5.1 Theory of Pressure Distribution Method for N_2 Measurement

The definitions of viscosity, the first and the second normal stress difference have been introduced in Section 2.2. A detailed demonstration of their relationship with the flow in the rotational rheometer will be presented in this section. The flow behavior of a material can be understood by studying the stresses generated in response to a specified flow field (stress-strain relationship) or constitutive equation. Typically, some simple flow velocity fields of the polymer melts and polymer solutions are made and the stresses are measured in experiments.

Figure 2.15 shows the ideal geometry for a cone-and-plate rheometer and the spherical coordinate system adopted. In most cone-and-plate rheometers, tips of the cones are truncated to avoid fluid vortex on these tips as indicated in **Figure 2.15**. It is thought

that the cone-and-plate rheometer will produce a simple shear flow in which the shear rate is very uniform throughout the flow field, when the cone angle is very small, say 4º or less, assuming no misalignment errors (Section 2.1). In the ideal cone-and-plate rheometer, the steady velocity field can be approximated in spherical coordinate as:

$$v_1 = \omega_0 r \frac{\theta - \frac{\pi}{2}}{\alpha}, \text{ and } v_2 = v_3 = 0 \text{ with } \frac{\pi}{2} < \theta < \frac{\pi}{2} + \alpha \qquad (2.\ 14)$$

Here the subscriptions and notations are listed below:

1 denotes the flow direction, ϕ (azimuthal angle);

2 denotes the velocity gradient direction, θ (polar angle);

3 denotes the neutral direction r (radial position);

ω_0 denotes the constant angular velocity of the cone (or plate);

α denotes the very small cone angle.

The uniform shear rate in an ideal cone and plate flow field is given as:

$$\dot{\gamma} = \frac{\omega_0}{\alpha} \qquad (2.\ 15)$$

Since the shear rate is homogeneous throughout the velocity field, components of the deciatoric stress tensor, $\ddot{\tau}$, are also independent of position in the cone-and-plate rheometer.

When the fluid fills the gap out to the radius R_0, the moment M exerted on the plate or cone surface is [45]:

$$M = 2\pi \int_0^{R_0} \dot{\gamma}\eta(R\cos\alpha)^2 \, dR = (\frac{2\pi}{3}) R_0{}^3 \dot{\gamma}\eta(\dot{\gamma})[1 + \mathrm{O}(\alpha_0{}^2)] \tag{2. 16}$$

Thus, measurement of the moment required to turn the cone or hold the plate gives a direct reading of the shear stress in the simple shear flow:

$$\tau_{12} = \tau_{21} = \dot{\gamma}\eta(\dot{\gamma}) = \frac{3M}{2\pi R_0{}^3} \qquad \text{when} \quad \dot{\gamma} = \frac{\omega_0}{\alpha} \tag{2. 17}$$

$\eta(\dot{\gamma})$ is the shear-rate dependent viscosity which can be described when the shear stress τ_{12} is divided by shear rate $\dot{\gamma}$ [45]:

$$\eta(\dot{\gamma}) = \frac{\tau_{12}}{\dot{\gamma}} = \frac{3M}{2\pi R_0{}^3 \dot{\gamma}} \tag{2. 18}$$

Assuming the velocity field is defined by Equation 2.5, the total stress tensor component, Π_{22}(r), is derived from the linear momentum balance equation in the radial direction [22]:

$$-\rho \frac{v_1{}^2}{r} = -\frac{\partial P}{\partial r} + \frac{2}{r}\tau_{33} - \frac{\tau_{11} + \tau_{22}}{r} + \frac{\partial \tau_{33}}{\partial r} + \frac{1}{r}\frac{\partial \tau_{23}}{\partial r} + \frac{\cos\theta}{r\sin\theta}\tau_{23} + \frac{1}{r\sin\theta}\frac{\partial \tau_{13}}{\partial \theta} \tag{2. 19}$$

As defined in simple shear flow, components of stress tensor are constant due to the homogeneous shear rate $\dot{\gamma}$,

$$\frac{\partial \tau_{ij}}{\partial r} = 0 \,. \tag{2. 20}$$

And $\tau_{23} = \tau_{32} = 0$ (2. 21)

because of the flow symmetry.

Thus Equation 2.19 can be simplified as [22]:

$$\frac{\partial \Pi_{22}(R)}{\partial \ln r} = (N_1 + 2N_2) \tag{2. 22}$$

Here it should be noted that an inertial or centrifugal force term is neglected as it is relatively small for high viscous polymer in a limited low shear rate range.

At the free boundary when $r = R_0$, approximating the boundary air/liquid interface as a partial sphere, the radial pressure exerted by the sample at steady state is atmosphere pressure P_0, which is the datum line of zero.

$$\Pi_{33}(R_0) = -P_0 \tag{2. 23}$$

A negative sign in Equation 2.23 arises because a compressive force is considered to be negative in the definition of the total stress tensor $\ddot{\Pi}$ as introduced in Section 2.2.

From the definition of the second normal stress difference N_2, Equation 2.22 can be expressed in the other form:

$$-\left(\Pi_{22}(R) + P_0\right) = -N_2 . \tag{2. 24}$$

With this boundary condition, integration of Equation 2.22 gives out the vertical stress profile expected to be present in homogeneous velocity field:

$$-\left(\Pi_{22}(r) + P_0\right) = -(N_1 + 2N_2)\ln\left(\frac{r}{R}\right) - N_2 \tag{2. 25}$$

Here R is the radius of the plate. The left hand side of Equation 2.25 is the net pressure acting perpendicular to the rheometer plate at radial position r. This quantity is measured with the miniature pressure sensors on the rheometer sketched in **Figure 2. 16**. Equation 2.25 is a very important relation that demonstrates the principles of the pressure distribution method. From Equation 2.25, the radical normal stress profile is expected to be linear in a semi logarithmic plot against a radial position if $\dot{\gamma}$ is homogeneous. The local normal stresses at various radial positions, the left side of Equation 2.25, are measured by the eight pressure sensors constructed on the rheometer plate. The details on the pressure sensor plate are described in Chapter 3 (Material and Equipment). Assuming that the measured local normal stress profile obeys the functional form predicted by Equation 2.25, both the first and second normal stress differences can be calculated by knowing the slope of the measured normal stress profile and the value of the local normal stress at the rim. The application of Equation 2.25 is demonstrated in **Figure 2.16**. The local normal stress at the rim can be calculated by extrapolating the local normal stresses profile values measured by the eight pressure sensors; thus the second normal stress N_2 is obtained. From the linear slope $-(N_1+2N_2)$ of the measured pressure distribution extracted from a semi logarithmic plot, the value of N_1 is obtained. Since the local normal stress is the net pressure exerted by the sample vertical to the pressure sensor plate, the total normal thrust F, exerted in the perpendicular direction on the plate can be calculated by integrating Equation 2.26 over the plate:

$$F = 2\pi \int_0^{R_0} -\left(\Pi_{22}(r) + P_0\right) r dr = 2\pi \int_0^{R_0} -\left(N_1 + 2N_2\right) \ln\left(\frac{r}{R_0} - N_2\right) r dr = \frac{1}{2}\pi R_0{}^2 N_1 \qquad (2.\ 26)$$

This is an alternative method to obtain the first normal stress, independent of N_1 measurement using the deflection of LVDT system.

It should be noted that, to get this relation several hypotheses were made:

(1). the shear rate is homogeneous throughout the velocity field of the sample filled between the gap;

(2). the flow field is symmetric,

(3). an inertial term and a centrifugal force terms is negligible,

(4). the air/liquid interface is exactly spherical and the flow on the boundary is exactly rheometric, and

(5). the surface tension at the liquid-air interface is negligible.

Assumptions (1) and (2) can usually be satisfied with sufficiently good alignment. The inertial error is negligible for viscous samples in rheometers with shallow cone angles. The error due to the centrifugal force can be corrected in an approximate way. The error of source (4) is probably less than 5% (Kaye *et al.*) [54].

2.5.2 Development of the Pressure Distribution Method

Since the 1970s there has been a general agreement on pressure distribution theory. When the rotational flow of liquids showing normal stress effects, the tension along the circular streamlines is always greater than that of other directions. So that the streamlines tend to contract, like stretched rubber bands, unless they are prevented by an appropriate pressure distribution.

Two types of measurement are possible by measuring the pressure distribution:

(1). determine the total force exerted on the whole plate by the liquid, from which the first normal stress difference N_1 is obtained and

(2). determine the local pressure distribution from the manometer or pressure transducers or pressure sensors reading, from which the second normal stress difference N_2 is obtained.

The striking advantages of this technique are:

(1). it is theoretically valid for a wide range of shear rates,

(2). it can measure all three material functions (η, ψ_1, ψ_2) simultaneously,

(3). it cross-checks the normal thrust data by comparison of the integration of the pressure distribution on the entire plate with the total thrust measured by a spring transducer,

(4). it does not require knowledge of the constitutive equation for polymer being tested.

In early studies of such a pressure distribution technique in polymer solutions, the plate of a cone-and-plate viscometer was drilled to provide tapping for manometers. Steady rotation of the cone results in the pressure distribution of the form indicated in **Figure 2.17**. This method might be used over a limited range of pressures at ambient temperature. Adam and Lodge (1964) [32] first used capacitance pressure gauges in small chambers linked by short tubes to a hole in the plate of cone-and-plate rheometer. Brindley and Broadbent (1973) [71] fixed 'Pitran' semiconductor pressure transducers set with their diaphragms in small cavities linked to holes in the plane of the plate of a cone-and-plate rheometer to make pressure distribution measurement on polymer solutions. Such methods are tedious and unsuitable if the properties vary with time because equilibrium is reached slowly. Furthermore, such methods cannot give a true pressure measurement because of the hole pressure error indicated in **Figure 2.8**.

Christansen and Miller [67] in 1971 made flush mounted miniature capacitance transducers to determine the pressure distribution in a cone-and-plate instrument and calculated the total force by integrating this pressure distribution. This was found to be equal to the spring measured force, thus obtaining a valuable check of the accuracy of this technique for the first time. Later on, Gao, Ramachandra, Magda, Baek and Lee [23,26,68-70] further explored this technique to measure the pressure distribution for various polymer solutions in cone-and-plate rheometer, as listed in **Table 2.1**. Although this flush mounted transducer plate was proven to be reliable in measuring the pressure distribution, other shortcoming came up. The plate needs to be so large (74 mm in diameter) because of the size limit of the pressure transducers that edge fracture (**Figure 2.18**) often occurs, which restricted the measurable shear rate range of the tested sample [72,73]. Consequently, the flush mounted transducer plate can often be used only at low shear rate.

The monolithic MEMS rheometer plate (25 mm in diameter) used in this thesis was fabricated with micromachining technology. This novel pressure sensor plate is able to not only measure the pressure distribution without hole pressure error, but also enables the measurement at higher shear rates up to 150 s^{-1} for a National Instrument Standard Test (NIST) standard fluid SRM-1490. In this thesis, the pressure sensor plate replaced the normal top plate and was used to measure the first and second normal stress difference of the silicone fluid PDMS. Because this plate can be used to measure the first normal stress difference without any LVDT transducers, it was also used to study the transient N_1 behavior of the standard NIST fluid SRM 1490 with and without presence of the LVDT so that the axial compliance error could be studied. The sources of these

materials will be presented in Chapter 3, along with the technical details of MEMS pressure sensor plate.

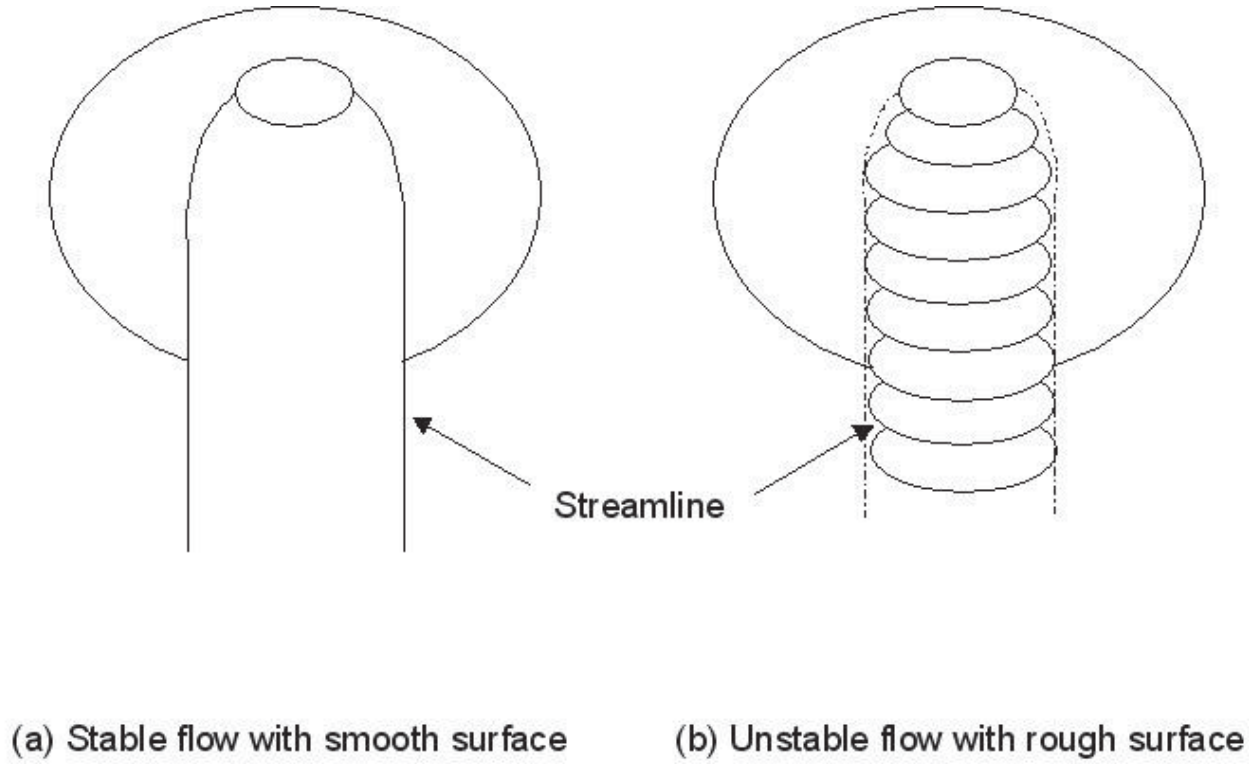

Figure 2.1. PDMS fluid through an extruder: the (a) stable fluid and (b) unstable fluid.

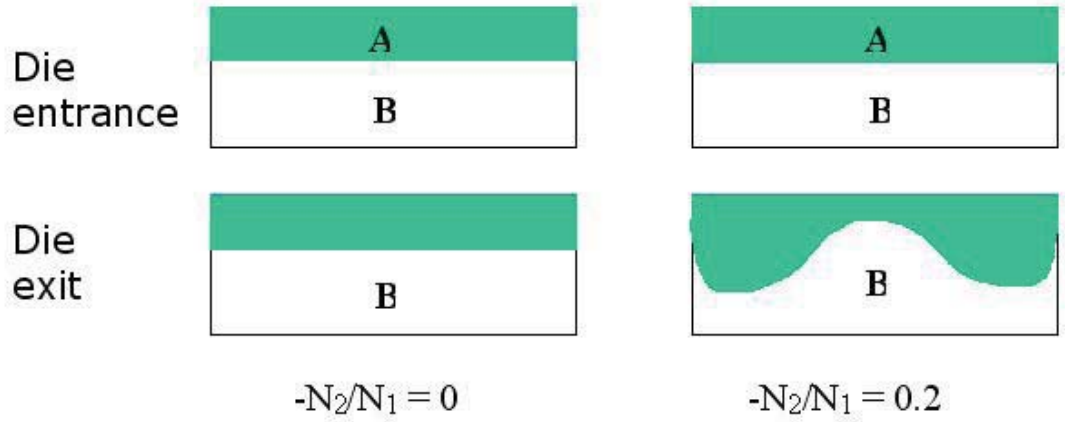

Figure 2.2. The interfacial irregularity of extrusion flow caused by the presence of the second normal stress (N_2).

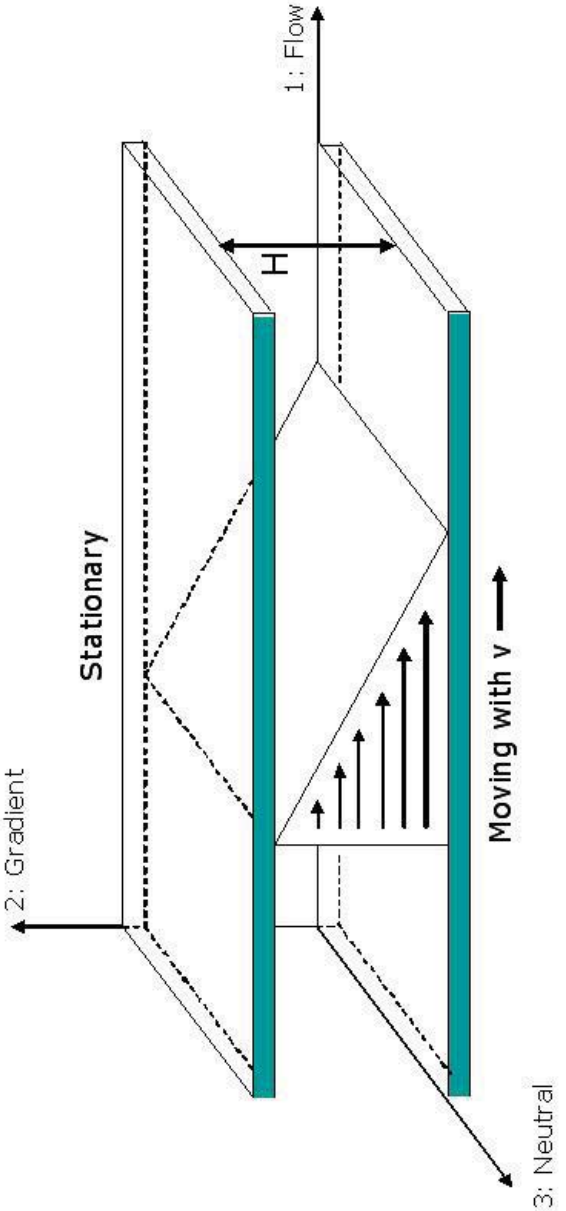

Figure 2.3. The simple shear flow between parallel plates, the bottom plate moving in velocity v.

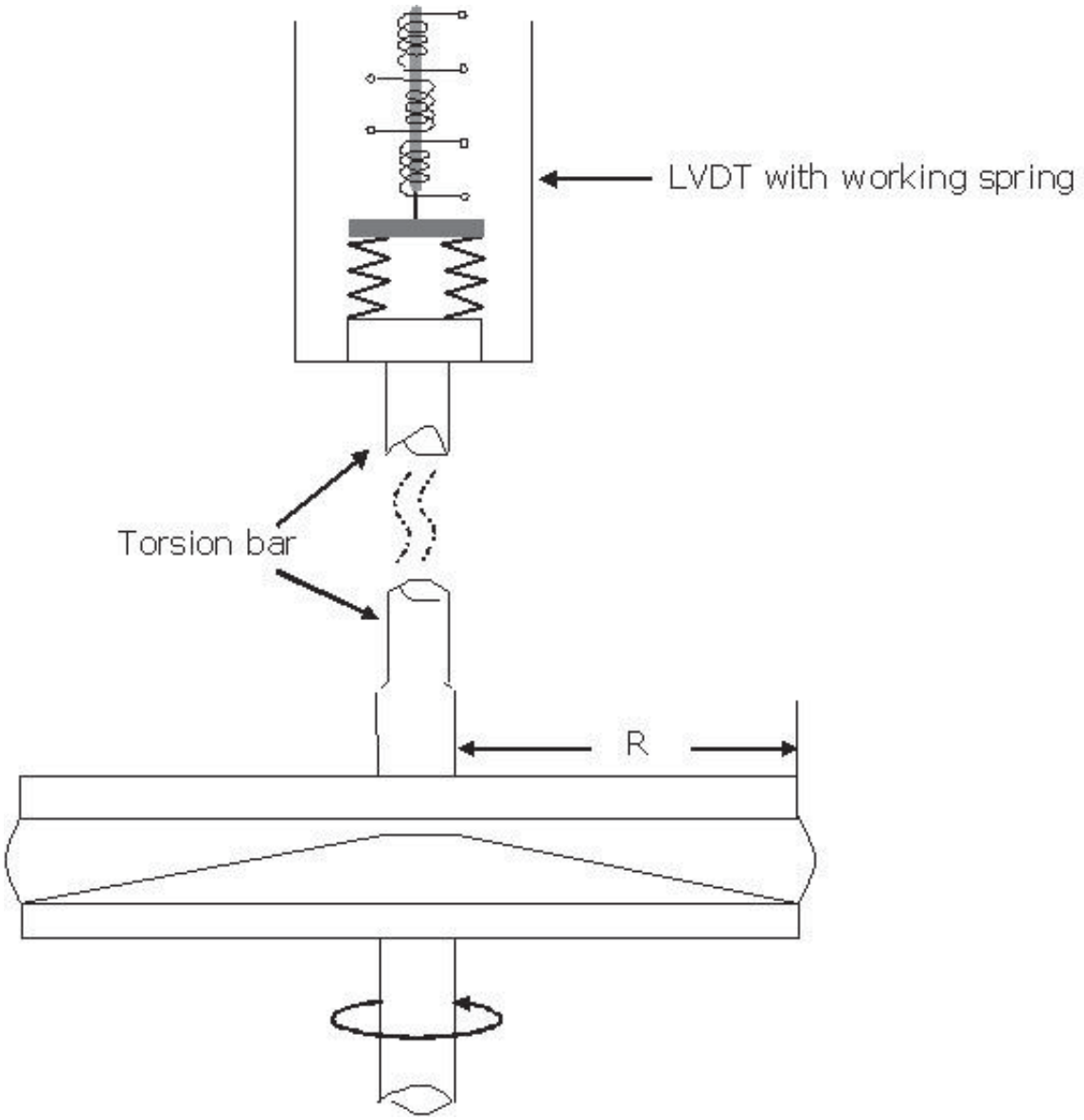

Figure 2.4. Schematic diagram of LVDT transducer working in the cone-and-plate rheometer.

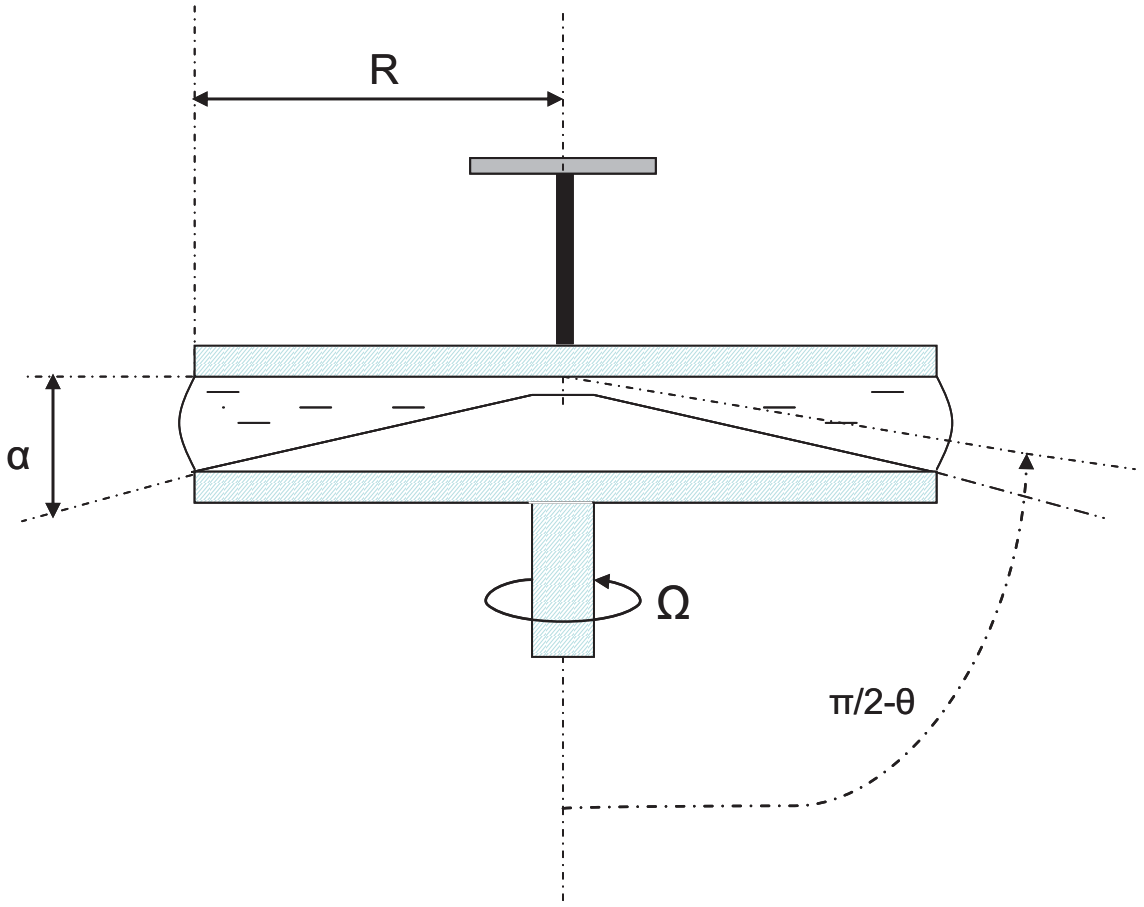

Figure 2.5. The spherical coordinates describing the flow field for the ideal cone-and-plate rheometer.

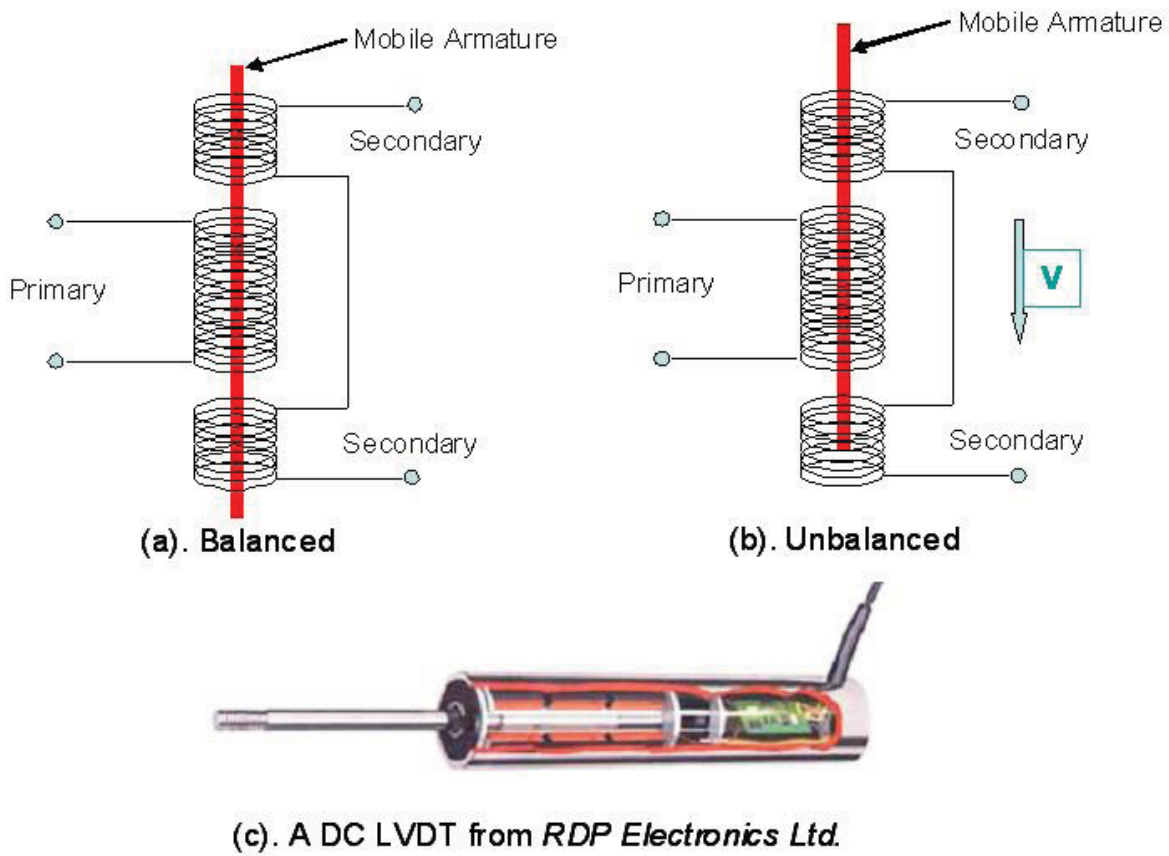

Figure 2.6. DC type of LVDT. (a) Balanced situation. (b) Unbalanced situation. (c) Commercially produced by RDP Electronics *Ltd.*

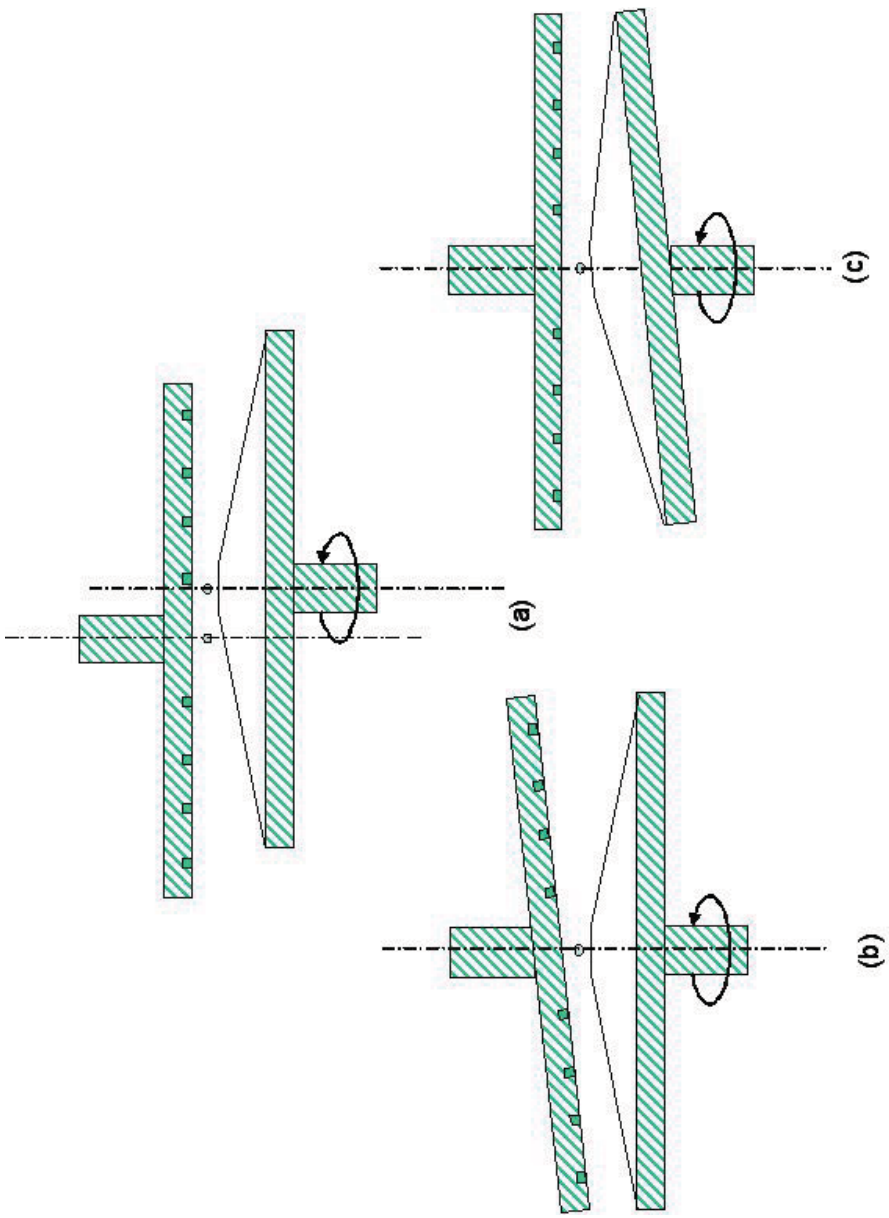

Figure 2.7. Misalignment illumination of the tilted plate and cone in the cone-and-plate rheometer.

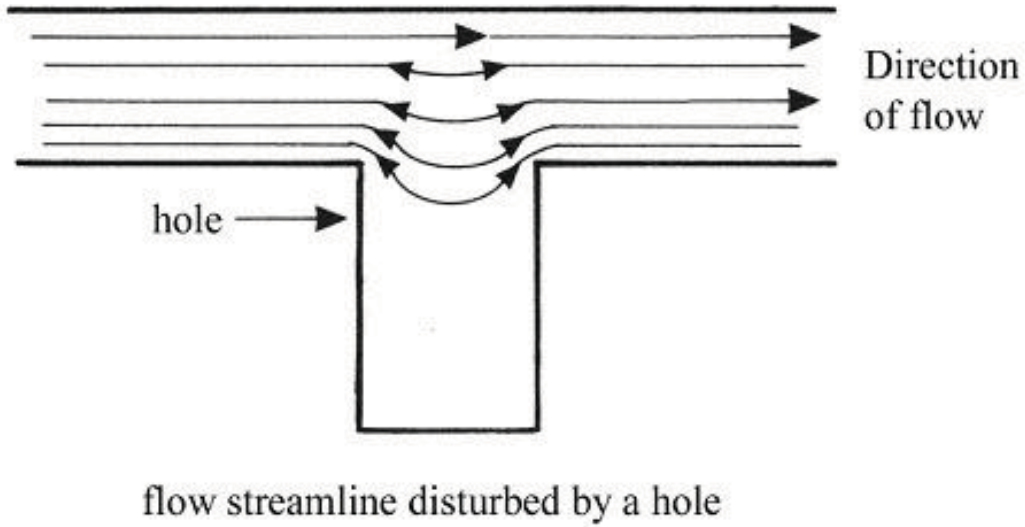

Figure 2.8. Schematic description of the hole pressure error.

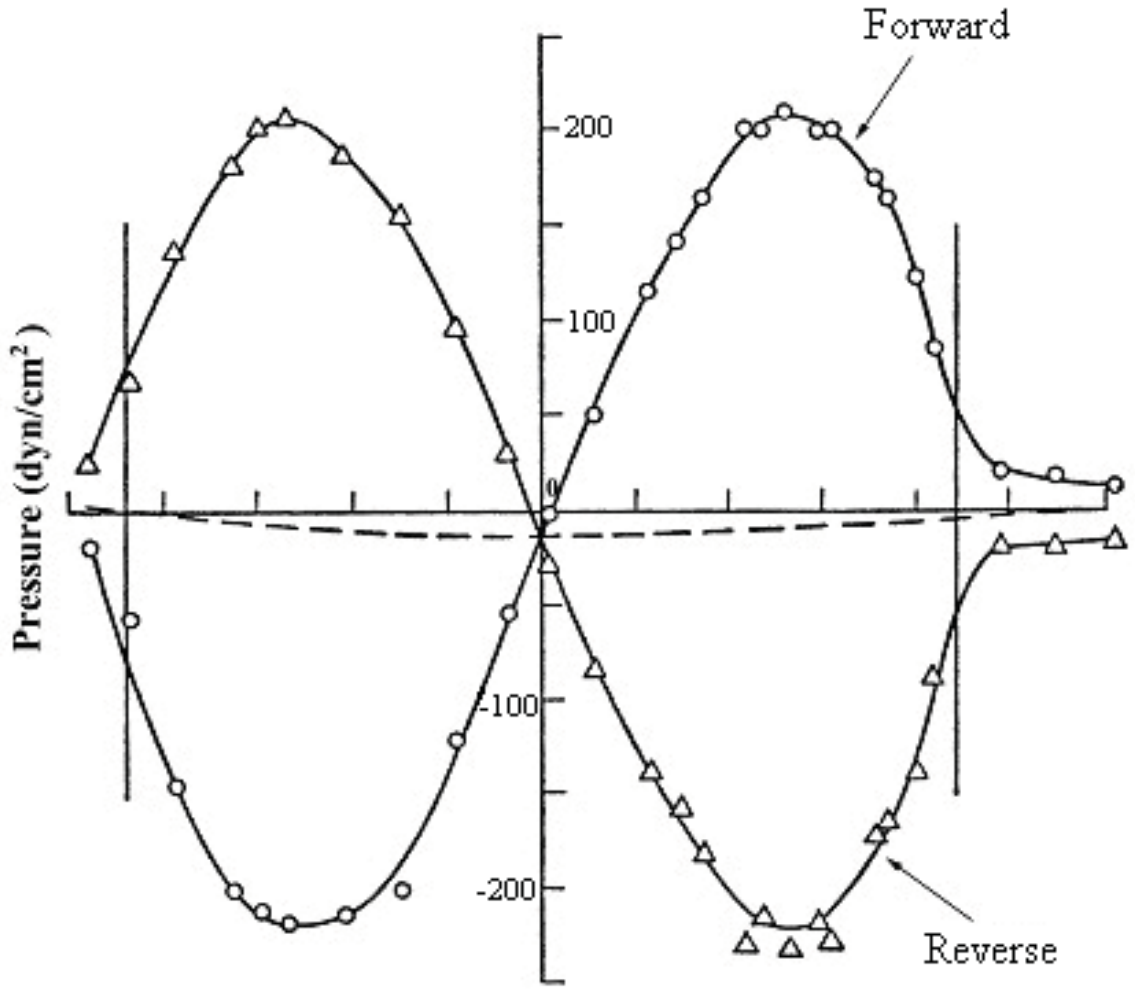

Figure 2.9. A diagramed description of the pressure distribution in tilted misaligned cone-and-plate rheometer (Adapted and simplied from Adams *et al.* [32] to show only pressure distribution in forward and reverse rotation manners)

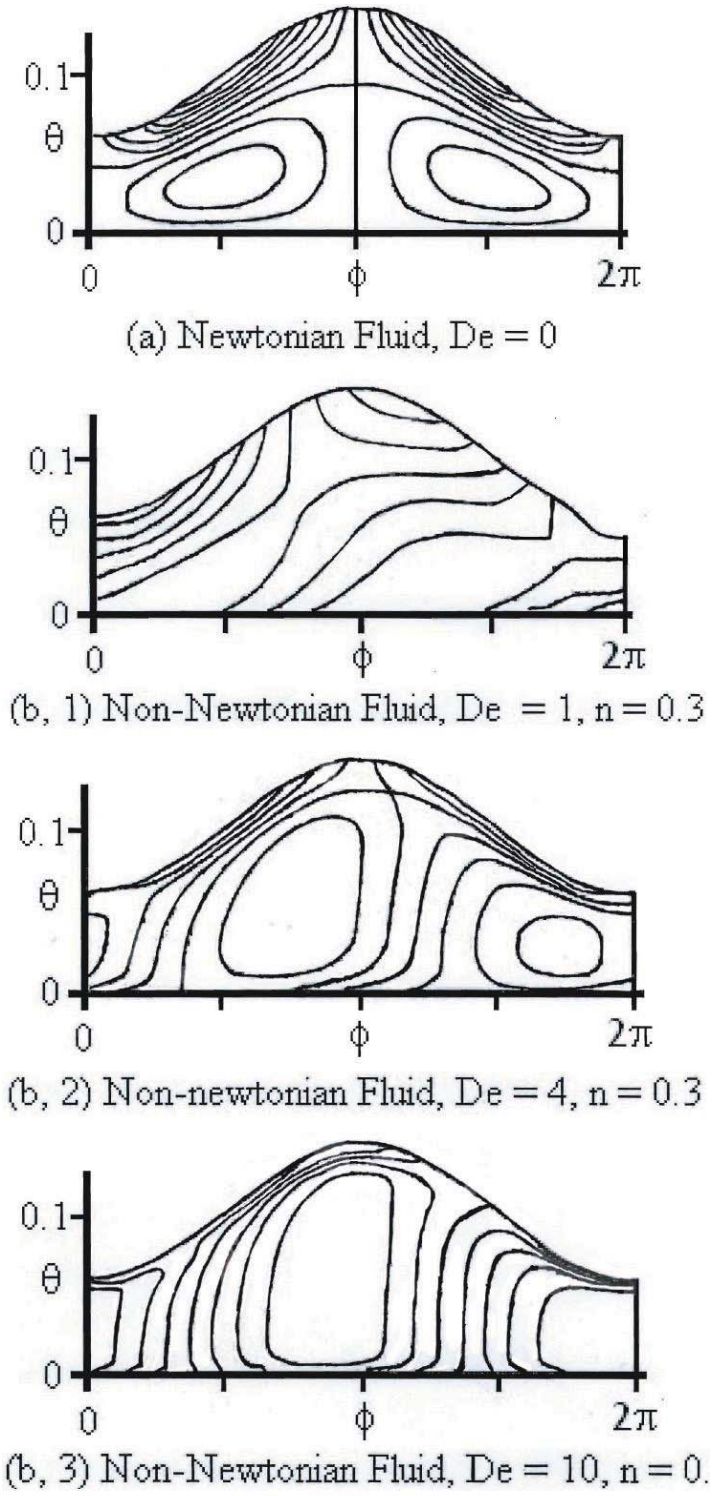

Figure 2.10. Description of the normal stress, $T_{\varphi\varphi,}$ distribution in tilted cone-and-plate rheometer with simulation. (Adapted and simplied from Dudgeous *et al.* [33] to show the local stress distribution)

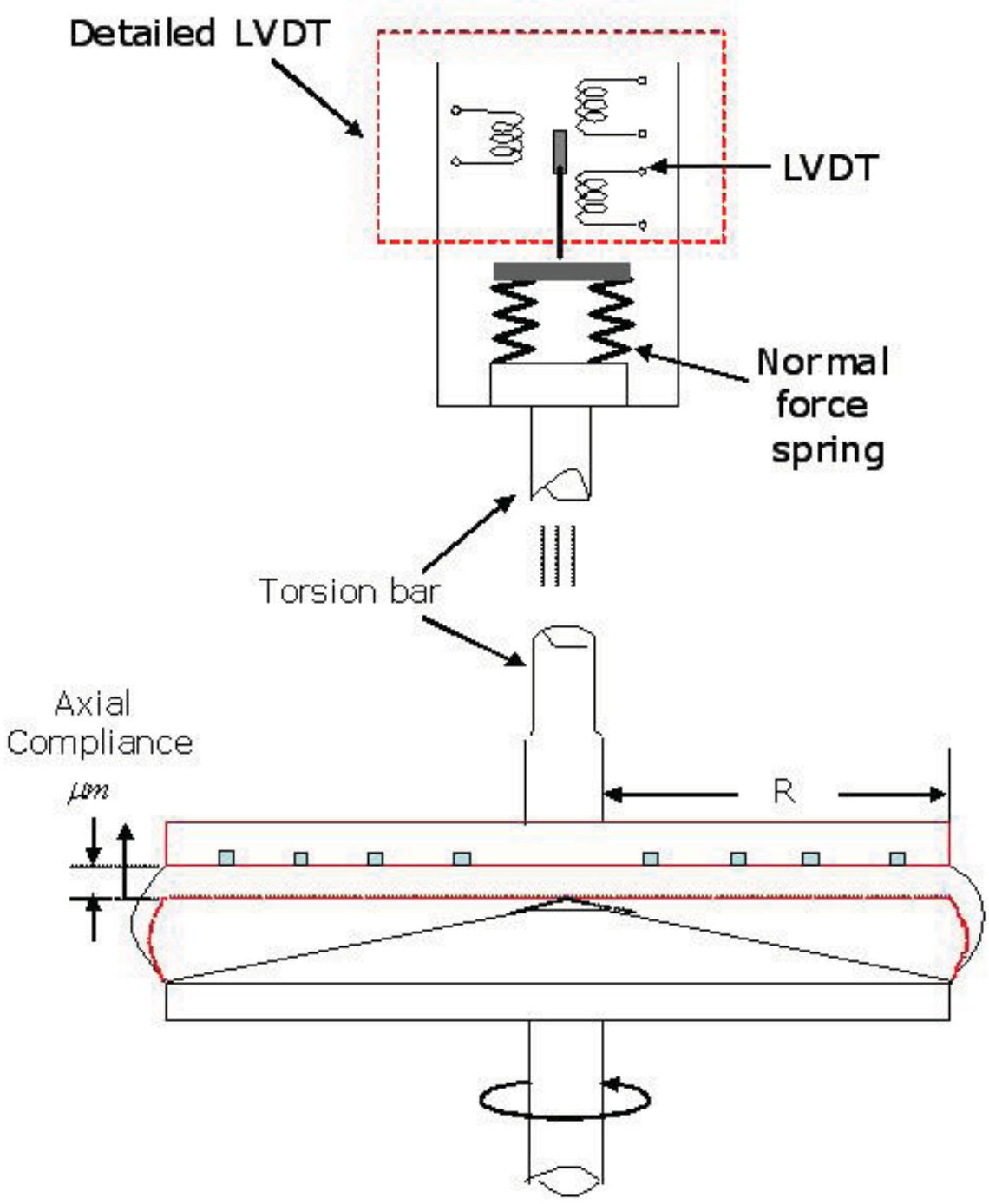

Figure 2.11. Schematic diagram of LVDT transducer working in the cone-and-plate rheometer.

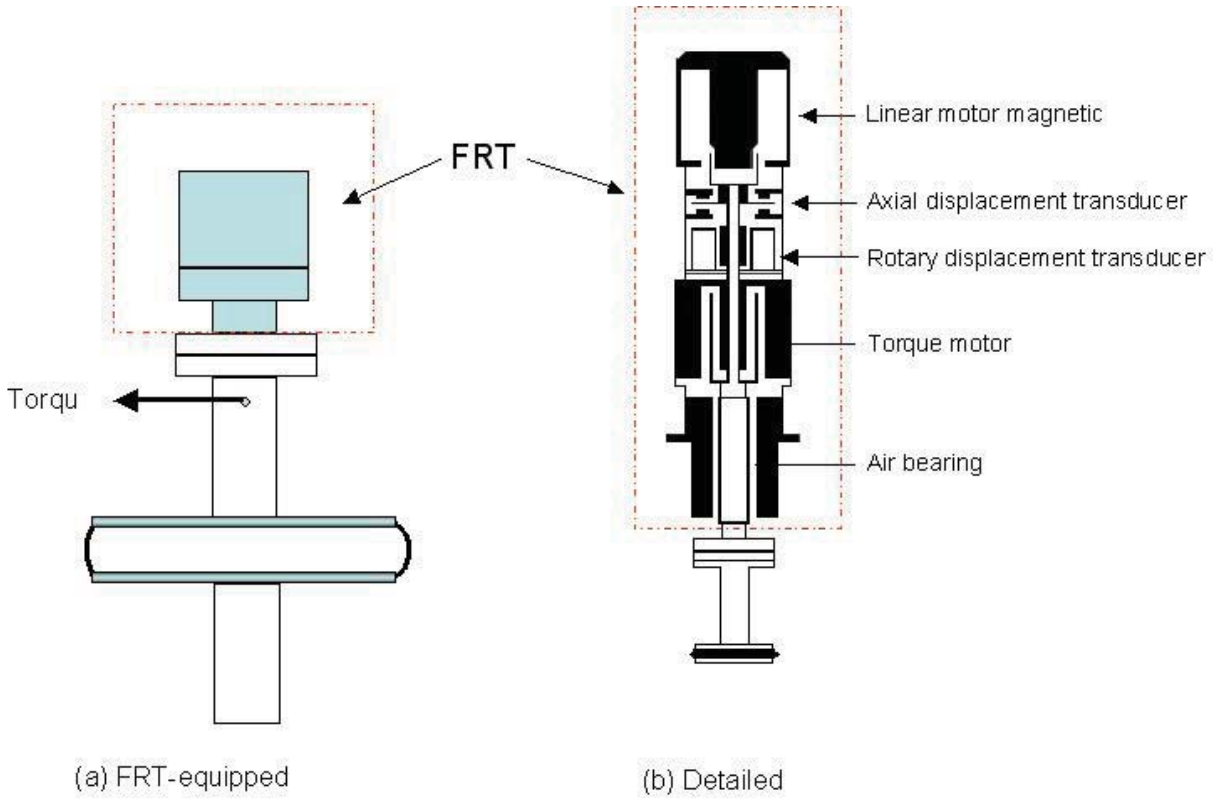

Figure 2.12. Schematic diagram of rheometer equipped with the force rebalance tranceducer (a) and detailed FRT (b).

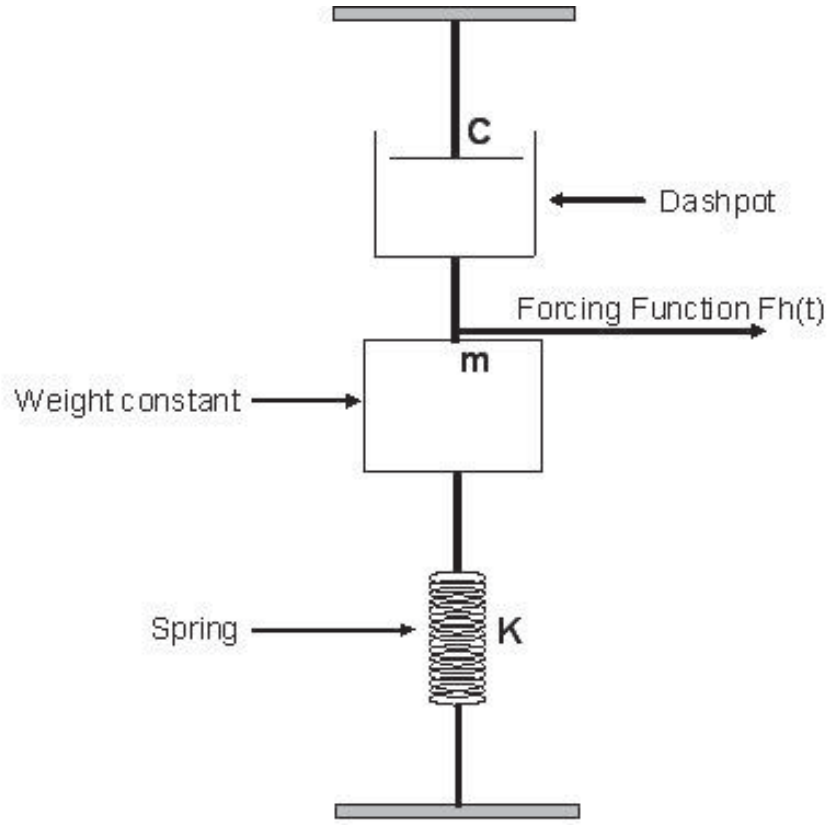

Figure 2.13. Stratton's test including inertia term, m, damping term, C, normal force spring, K, and force function Fh(t).

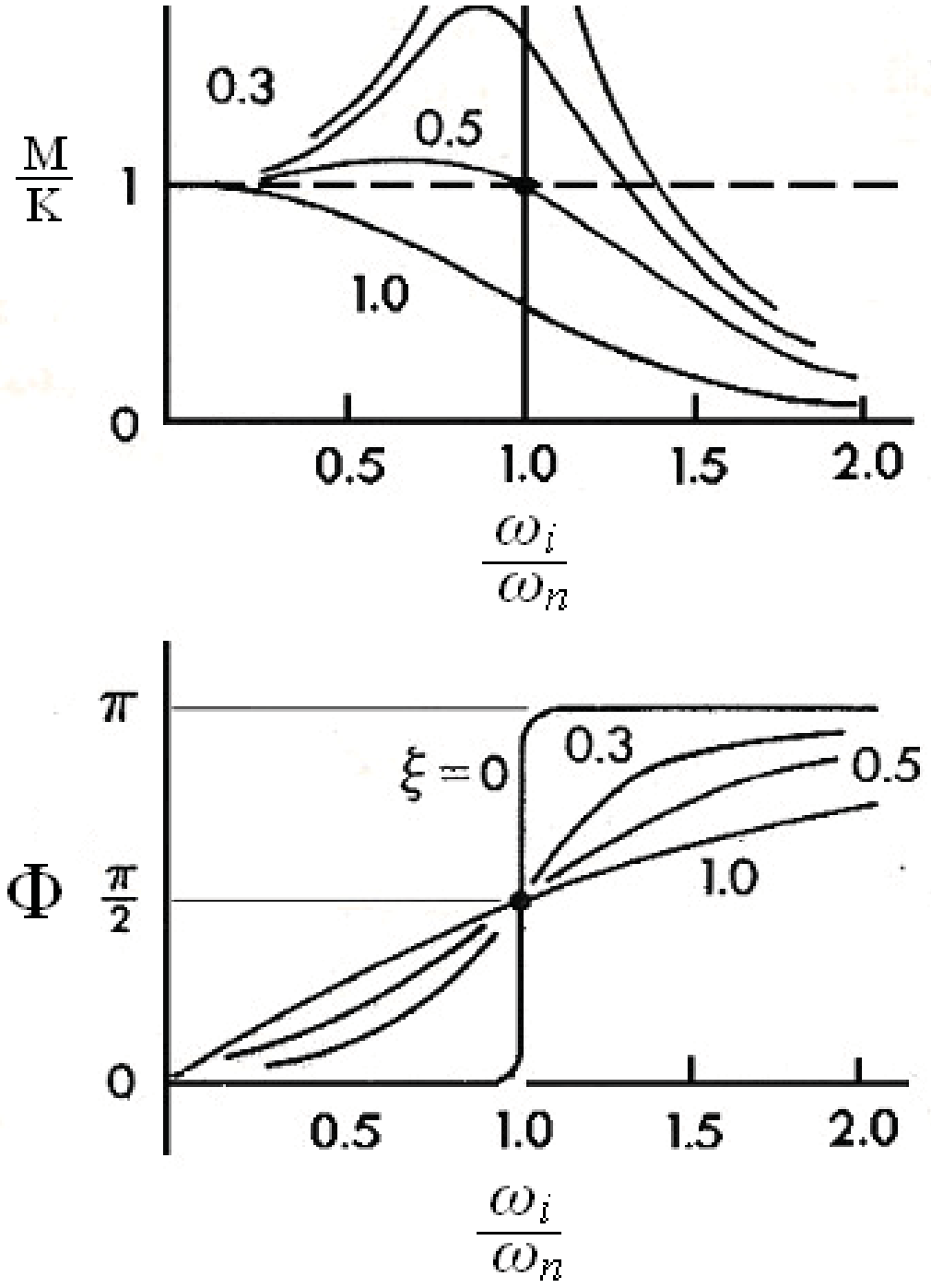

Figure 2.14. The frequency response of the 2nd order instruments.

Table 2.1. Prior investigations of the normal stress difference coefficient ratio, ψ

Method #	Description of method	Investigators	Fluid studied	Shear rate (s^{-1}) range	$\psi = -\frac{N_2}{N_1}$
1	Annular flows	Hays and Tanner [27]	Poly-(methylmethacrylate) in toluene	-	very small
		Huppler [47]	aqueous polymer solution	1500	(-0.20, -0.06)
2	measure expansion of a jet of fluid from a capillary	J.L.White and A.B. Metzner [48]			
3	free surface measurement of a fluid flowing down an open channel	M. Keentok et al [49]			
		Kuo and Tanner [50]	5.4% poly(isobulene) in cetane	750	<0
4	onset of Taylor instabilities in Couette flow	Den et al. [27]	various dilute polymer solution	-	>0
5	the difference in total thrust measurements between cp and pp rheometer	Ginn and Metzner [46]	5.09% poly(isobutylene) in decalin	500	(0, 0.26)

Table 2.1 continued

		Berry and Batchelor [51-52]	(a).Depolymized natural rubber	0.324	(0, 0.1)
			(b).bulk polyisobutylene	0.229	(0, 0.1)
		Kaye, Lodge, and Vale [53]	2% poly(isobutylene) in a low mw Poly(isobutylene)	25	(0, 0.07)
6	Total force difference of pp and cp with tip of cone separated from plate	Jackson and Kaye [54]	5.66% high mol. Wt. poly-(isobutylene) diasolved in low mw poly(isobutylene)	3	0.5
7	total thrust as function of separation of cone and plate, cp	Marsh and Pearson [55]	(a). 0.9% HEC in water	850	(0.07,0.15)
			(b). 2.5% polystyrene in arodor	170	0.2
		N.Ohl and W.Gleissle [56]	(a). Pure polyisobutene	0.5	(0.1, 0.2)
			(b). 34.5% limestone in polyisobutene		(1, 3)
8	the capillary and slit die rheometer				

Table 2.1 continued

9	optical flow birefringence measurement	E. F. Brown et al. [57]	low polydispersity poly- styrene in tricresyl phosphate	15	0.23
10	hole pressure error measurement in flow over slots	D.S.Malkus et al. [58]	estimation	-	
		E.A. Kearsley et al. [59]	6% polyisobytylene in Mentor 28		0.22
13	measuring the normal force and the air bubble pressure in the cone-and-ring or plate-and-ring rheometer	Harris Van Es [60]	a 5% solution of polyisobutene in decalin (1) and a silicone oil (2)		>0
14	the ratio of normal force measured by modified cone and partitioned plate	J. Meissner et al. [61]	low density polyethylene (LDPE)	0.5	0.24
		H.Egger and P. Schummer [62]			
		T.Schweizer [63]	Polystyrene	30	(0.05, 0.24)
15	measurement of the free surface rising height near a rotating rod (rod climb-ing method)	J.Z.Lou [23]	0.1% Polyisobutylene in oligomeric poly-butene(Boger fluid)	Very low	-0.01 ± 0.01

Table 2.1 continuted

		G.S. Ribeiro et al. [64]	heavy crude oils	Very low	
			(a). Lakeview	-	0.21
			(b).CND	-	0.2
			(c).Zuata	-	0.1
		L. Di Landro et al. [65]	Poly(dimethylsiloxane)* (PDMS)	Very low	(0.056, 0.189)
16	fllush mounted pressure tranducers (pressure distribution method)	E.B.Christiansen and W.R Leppard [66]	2.5% polycrylamide solution	100	(0.05, 0.1)
		M.J. Miller et al. [67]			
		J.J. Magda et al. and K.L.DeVries [68]	0.1% Polyisobutylene in oligomeric poly-Butane (Boger fluid)		0.3 ± 0.01 for star polymer
					0.21 ± 0.01 for linear polymer

Table 2.1 continuted

		Lee et al. [69]	21.5% polyisoprene in Tetrandecane		0.29
		J.J. Magda and S.G. Beak[70]	8% polystyrene in *n*-Butylbenzene		0.275
17	MEMS micro-pressure sensor plate (pressure distribution method)	S.G. Beak and J.J.Magda [44]	NIST SRM-1490	150	0.10 ± 0.02
		M.B. Lee et al. [26]	Polydimethylsiloxane * (PDMS)	10	

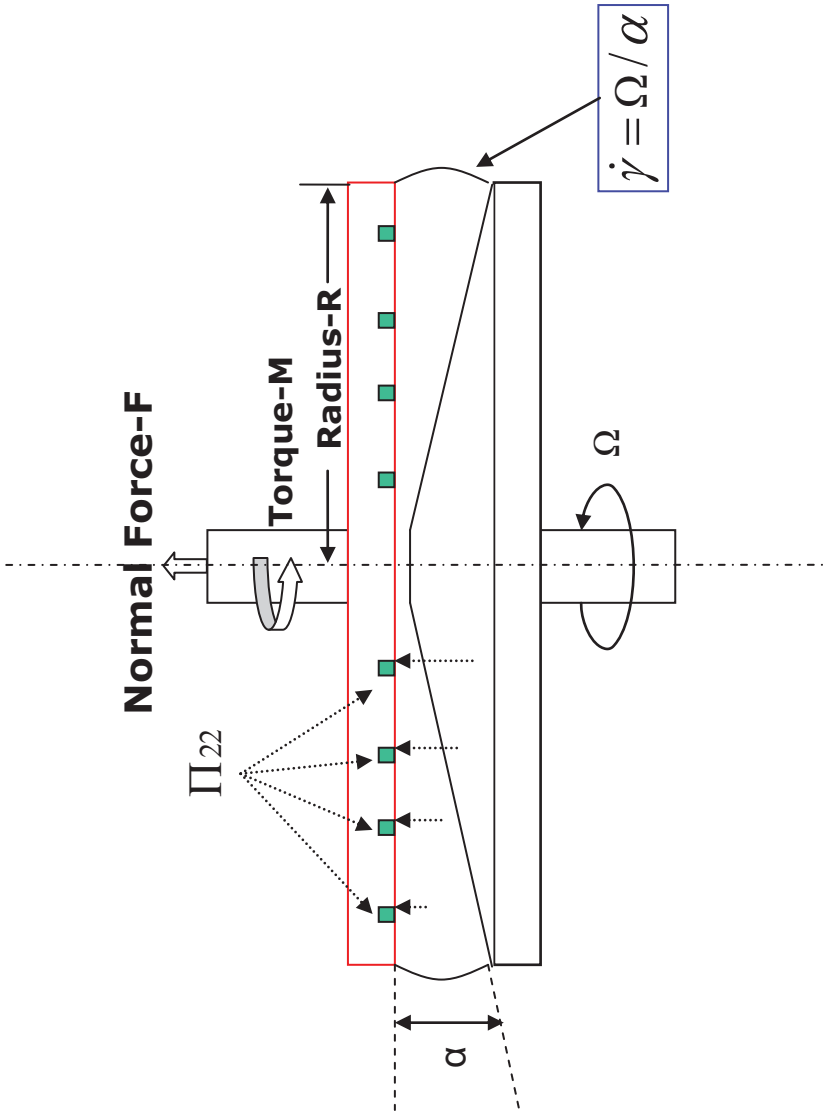

Figure 2.15. Diagramed description of the ideal geometry of cone-and-plate rheometer.

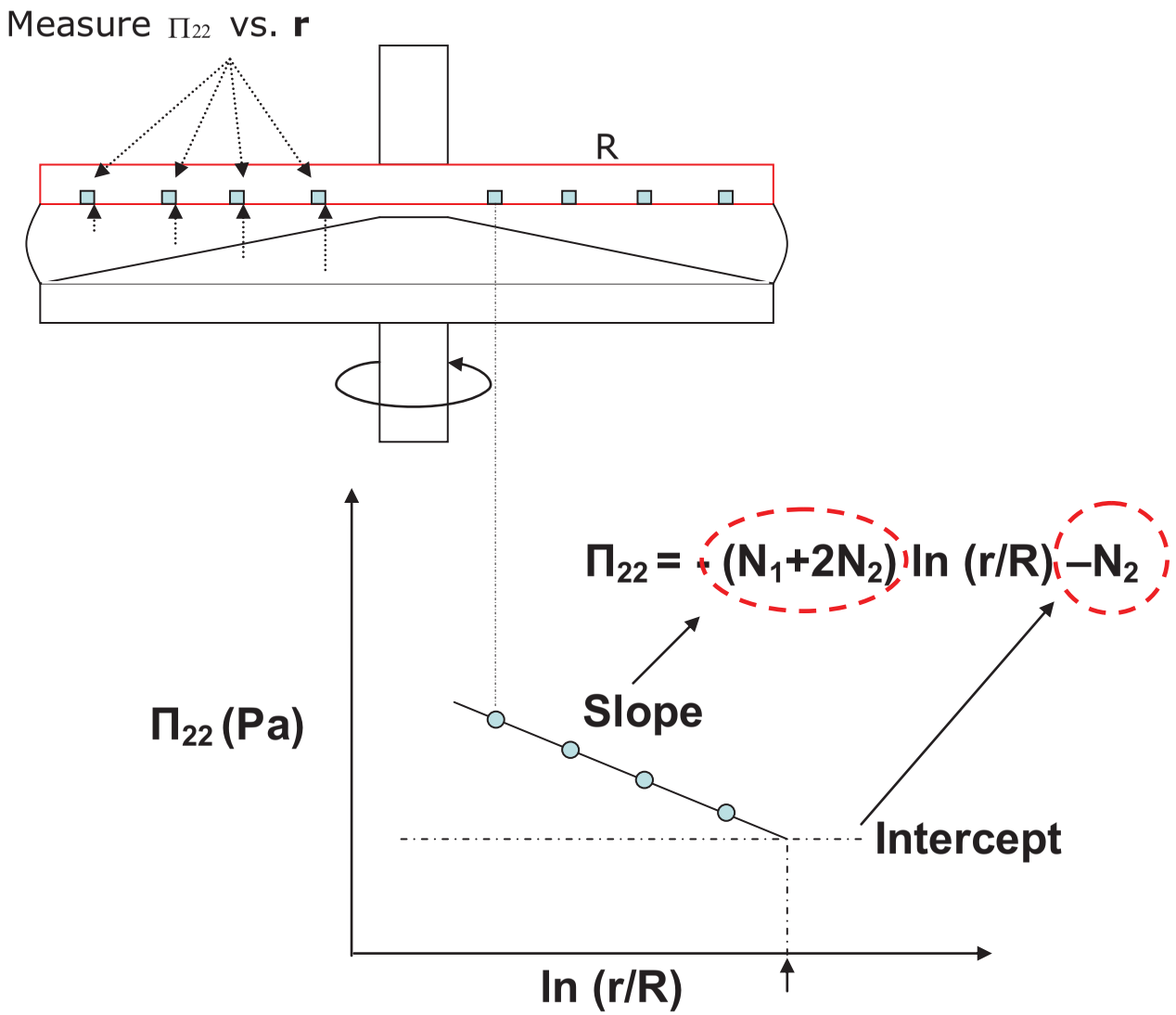

Figure 2.16. Diagramed descriptions of the tenses along the circular streamlines.

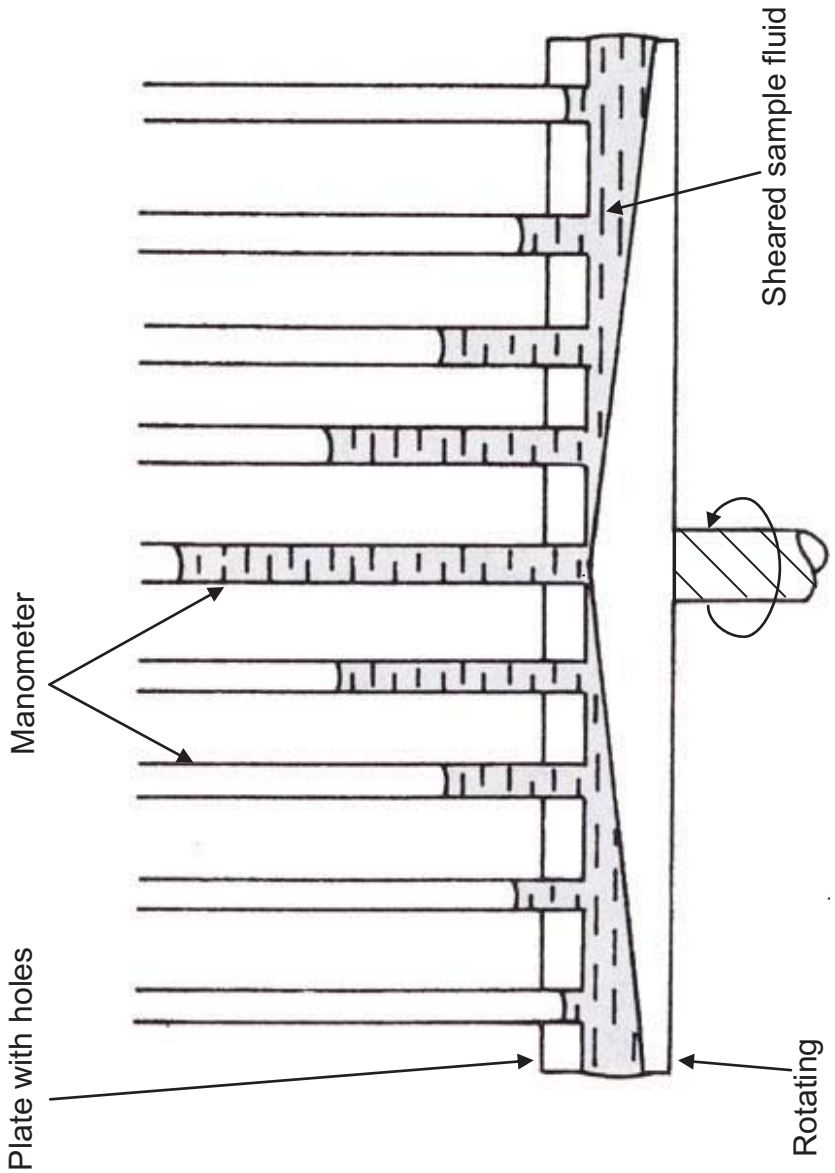

Figure 2.17. Prototype of manometer plate used for early study of pressure distribution.

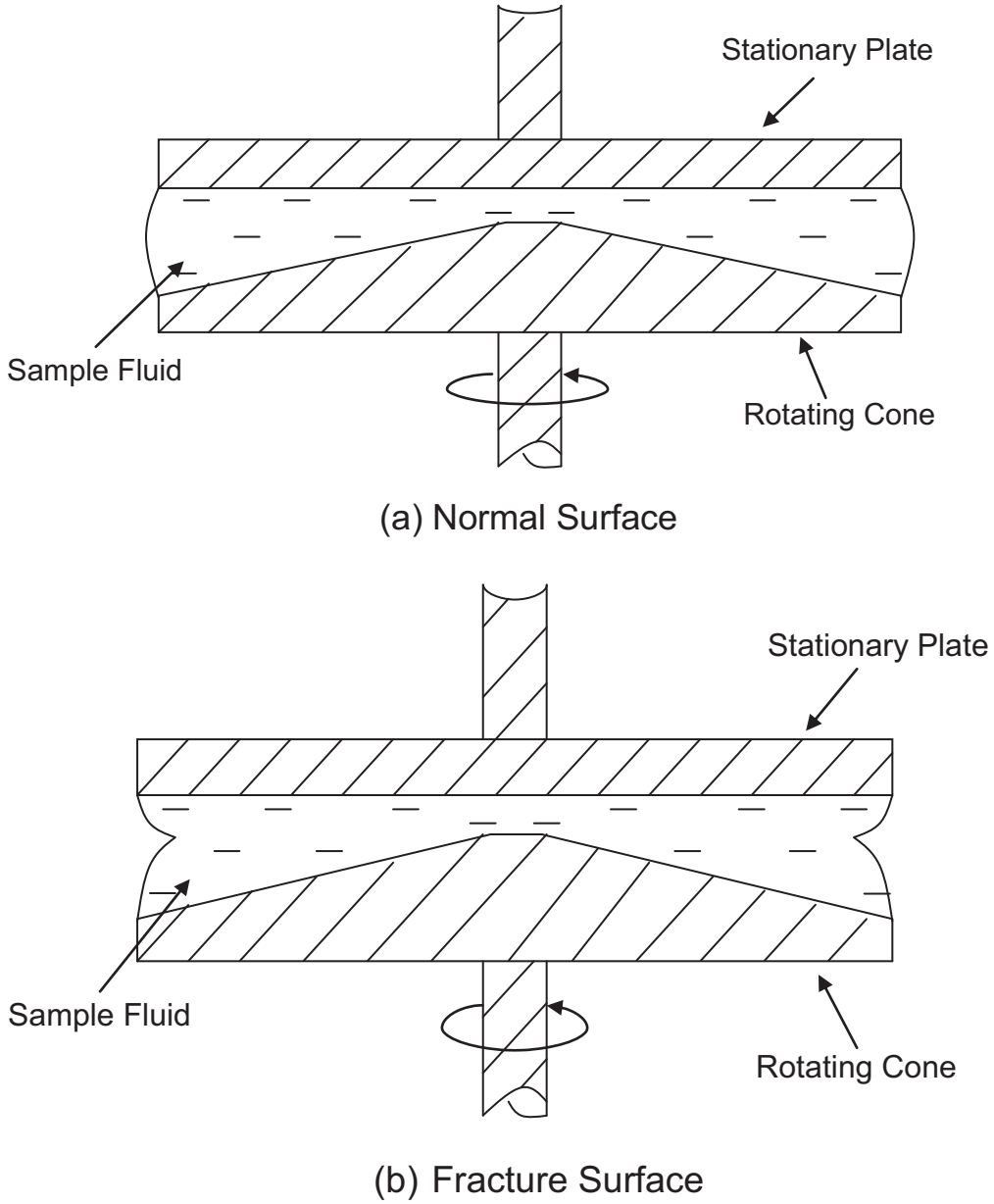

Figure 2.18. Schematic diagram of edge fracture for a cone-and-plate rheometer: (a) normal surface and (b) fracture surface (The sample is shear between the cone and the plate).

CHAPTER 3

MATERIALS AND METHODS

3.1 Introduction of the Material Used in This Thesis Work

Two different polymer materials were used in this research for different purposes. This work is more focused on the study of accuracy of the rheological measuring system than on the materials. As a matter of fact, both materials are used as testing fluids to detect abnormal behavior due to the imperfections of the measuring system. The pure polymer melt of PDMS (polydimethylsiloxane) was tested for the start-up behavior of the first normal stress differences N_1 in order to detect the effect of the natural frequencies of transducers: LVDT and the capacitance pressure sensors. In addition, the first and second normal stress differences, N_1 and N_2, of the PDMS were measured. A standard NIST fluid SRM 1490, a polymer solution, was tested separately with and without the LVDT in effect in order to study the influence of the axial compliance due to the finite stiffness of the LVDT system.

3.1.1 PDMS

Silicone fluids PDMS, polydimethylsilaxane, (molecular structure shown in **Figure 3.1**) are commercial polymer melts. They are transparent liquids at ambient temperature and have remarkable mechanical, chemical, and thermal stabilities from low temperature -70 ^{o}C up to as high as 250 ^{o}C. Because they can be used without heating,

PDMS is easier than other polymer melts for rheology testing at room temperature. PDMS fluids are available over a wide molecular weight range from Newtonian fluid to elastic Non-Newtonian fluid with viscosities in the range of from 5 cps up to 300,000 cps [74]. Non-Newtonian PDMS fluids exhibit shear-thinning (**Figure 3.2**). Shear thinning is defined as the viscosity decreasing with increasing shear rate. The disentangling of the linear polymer molecules can be the main cause of this phenomenon.

PDMS was originally developed to be used as a dielectric coolant and as a solution in solar energy installations. In general, PDMS is widely used in coating, seals, gaskets, adhesives, and medicine [75]. Its importance arises in medicine because of its resistance to blood fluid as described by *Allcock et al.* (1981) [76]. Due to the versatility of the material, PDMS has been widely studied corresponding to different applications [77-81]. On the other hand, the studies relevant to the processing of the PDMS product are not complete. As a matter of fact, it is essential to know the rheological properties of PDMS, i.e., viscosity, the first and the second normal stress differences for the proper operation of the industrial processing or other applications that involve this material. Studies of the rheometry of similar types of shear-thinning polymer fluids have been carried out (see **Table 2.1** for reference), and these studies have an important role on the developing rheological knowledge of PDMS. For example, the reptation model has been developed to predict the first and second normal stress difference for linear polymer melts, and has been proven to be quite successful in describing many experimental results [23] in the linear viscoelastic or very low shear rate regime. Based on the reptation theory, the normal stress ratio of the PDMS is predicted to be between 0.12 and 0.17. The only experimental measurement of the second normal stress difference for PDMS was

done by Di Landro *et al.* (2003)[65]. Di Landro's group measured the low-shear viscosity (η_0) and the first normal stress difference coefficient (ψ_1) of a series of linear PDMS of different molecular weights with a rotational rheometer, and they also measured the second normal stress difference coefficient with the use of a rotating rod apparatus (method listed in **Table 2.1**). Based on the experimental measurement, the normal stress ratio, $\psi = -\frac{N_2}{N_1}$, differed with molecular weight of the PDMS fluid. The measured normal stress ratio of non-Newtonian PDMS fluid (PDMS 600) turned out to be between 0.141 and 0.154 at room temperature, 20 °C. In this thesis work, the pressure distribution method was used to measure the second normal stress difference is the non-Newtonian linear PDMS fluids, kindly supplied by Rhodosil (FITZ CHEM CORPORATION 450 E. Devon Suite 175 Itasca, IL 60143). This sample was used as received; its nominal viscosity value is 300 Pa-s.

3.1.2 NIST Fluid SRM-1490

S.R.M/R.M. stands for standard reference materials/reference materials [82]. Standard reference materials and reference materials are issued by NIST (National Institute of Standards & Testing, Gaithersburg, MD) to address needs of the producers, processors and users of polymers for calibration and for performance evaluation of instruments used in the control of the synthesis and processing of polymers as well as benchmarks for comparisons of measurement methods and development of new materials.

The polymer solution SRM 1490 is one of the Nonlinear Fluid Standards, which is composed of a high-molecular mass poly-isobutylene dissolved in normal hexadecane.

Non-Newtonian rheological standards are developed to exhibit the typical polymeric behaviors of shear thinning and normal stresses; these standards are also used for calibration of rheological instruments and for research into improved measurement methods. Polymer fluids, such as polymer melts and solutions, often do not follow the simple Newtonian ideal in their flow behavior, demonstrating shear-rate dependent viscosities and normal stresses. Such fluids see wide application in everyday life (injection molding, paints and coatings, food products, etc.), and the ability to measure and characterize their behavior accurately is very important to optimizing their processing conditions. Since there are a number of commonly used methods to measure the flow behavior of polymers, the Standard Reference Material (SRM 1490) will provide a way for comparing the performance of different instruments, as well as providing tools for research into better methods of measuring the rheological properties of polymeric fluids. SRM 1490 is certified for the shear-rate dependence of viscosity and first normal stress difference at temperatures of 0 ºC, 25 ºC and 50 ºC. The linear viscoelastic responses are also certified, along with the temperature dependence of the shift factors. However, NIST does not certify N_2 values for SRM-1490 or any other standard fluid. SRM-1490 is no longer available because it has been replaced by SRM-2490 at NIST.

3.2 Instruments

3.2.1 Weissenberg R-17 Rheogoniometer

The Weissenberg R-17 Rheogoniometer is a standard torsional rheometer with two LVDT measuring system (Section 2.2), one for the torque and one for the normal force. The normal force measuring system uses a light spring with a very sensitive spring constant ($\approx$1000 $dyne/\mu m$). In this thesis, the cone-and-plane geometry of Weissenberg

R-17 Rheoginiometer was combined with the pressure sensor plate to explore the behavior of the silicone fluid PDMS in the presence of an unavoidable degree of cone and plate misalignment. The Rheogomiometer was also used to test the transient start-up N_1 response of PDMS in the presence of the LVDT axial compliance.

Three cones with different cone angle were used in this study. The tips of the cones were truncated in order to prevent the clustering of the sample at the touching point of the cone tip and the plate. Details such as cone diameters, cone angles and the truncated distances of the cones are summarized in **Table 3.1**. The angular velocity of the cone was controlled by a gear-motor system with a 60 variable speed and ranging the shear rate from 1918.2948 per second to 0.0242 per second [29]. LVDTs with the normal force spring and a torsion bar were used to measure the total normal thrust, F and the torque, M, respectively. In this procedure, instrument compliance errors were involved in both measurement of normal force thrust and torque (Sec. 2.4.2). Alternatively, the novel pressure sensor plate was used to measure the normal thrust. It should be noted that axial compliance was still present due to the deflection of normal force spring in the LVDT transducer.

The data acquisition system is sketched in **Figure 3.3**. Firstly, the LVDT transforms the displacement of the torsion bar or normal force spring into electronic signals (in volts). These electronic signals were magnified by two transducer-meters (Boulton-Paul Aircraft Company, Model EP-597M, S/N 1027&1089). The amplified signals were transmitted from the transducer-meters to a data acquisition board (NI 6023E Multi-function Data Acquisition Board, National Instruments Corporation, Austin, Texas). The board has a 12-bit analog-to-digital converter with 16 analog input channels

at 200 kS/sec sampling time, and is connected to a personal computer. As the electronic signals were detected by the DAB, they were digitized, and then logged by a commercial software package Virtual Bench – Logger, Version 2.6 (National Instrument Corporation, Austin, Texas), and finally displayed as the analyzable data (in volts).

The calibration of the signal collecting system is required before every rheology experiment in order to assure a normal working condition. The calibration procedure is to check the torsion bar constant and spring constant using static weights [29].

According to the instruction manual of the Weissenberg rheogoniometer, from the measured torque, the viscosity of the test fluid can be calculated as:

$$\eta = \frac{\tau_{12}}{\dot{\gamma}} = \frac{M}{\pi r^2 \dot{\gamma}} \tag{3. 1}$$

The torque exerted by the sheared sample on the upper plate can be measured by a torsion bar which has a spring constant K_T . The spring constant of the torsion bar, K_T is expressed in the equation as follows:

$$K_T = \frac{M \times V_f}{R_g \times V} = \frac{2 \times l \times g \times m \times V_f}{R_g \times V} \tag{3. 2}$$

Here, g is the gravitational constant (980 cm/s^2), m is the applied standard mass in gram, R_g is the measurement range set on the transducer meter in μm , V_f is the full-scale voltage of the transducer meter, and V is the measured voltage signal by LVDT system correspondent to the applied torque, l is the effective length of the moment arm of the calibrating fixture. Ideally, K_T is constant; however, due to the different sensitivity of the various ranges, signal noise would affect measurements, thus causing a deviation.

A special fixture (**Figure 3.4**) was designed and fabricated for the torque calibration. By hanging two standard weights on the end of the monofilaments, and simultaneously with the use of the pulleys, part of the air bearing which connect the top plate with the torsion bar was twisted and a torque with known value could be detected and measured (as V in eq. 3.2) by the torsion bar. The length of the momentum arms of this fixture, l in eq. 3.2, is fixed as 7.57 cm. The values of the calibration constant of torsion bar K_T were calibrated in different voltage ranges (V_f in Eq. 3.2) and averaged throughout all the measuring ranges. The averaged value of the calibrated constant of the torsion bar was 14860.5 ± 714.3 $dyne \cdot cm/\mu m$. This value is close, by 2% of deviation, to the manufacturer's reference value.

The spring constant of the spring in the normal force measuring system, K_N, can be expressed similarly as Eq 3.2 as:

$$K_N = \frac{F \times V_f}{R_g \times V} = \frac{m \times g \times V_f}{R_g \times V} \tag{3. 3}$$

m is the applied standard weight in gram, g is the gravitational constant, R_g is the measuring range set on the transducer meter in μm, V_f is the full-scale voltage of the transducer meter, and V is the measured voltage signal by LVDT system correspondent to the applied normal thrust.

The normal spring constant was calibrated using standard weights (m in eq. 3.3). Total normal trust was applied on the top plate by placing standard weights on the top of the tope plate holder. The induced LVDT voltage V was measured via the transducer meter at a certain measuring range V_f. The normal spring constants at different

measuring ranges of the transducer meter were calculated using Eq. 3.3. The averaged value of the normal spring constants was 806.6 ± 19.8 $dyne/\mu m$. The value has a apparent discrepancy with the manufacturer's value, by 20% of deviation. The change in K_N value may be caused by the use of a new transducer meter (S/N 1189).

The cone and plate were aligned to be as concentric and parallel as possible using a dial gage indicator (Mitutoyo Truetest Test Indicators - Series 513, Automation & Metrology Inc.). The concentricity axis was adjusted to be less than 0.0005 in and the flatness less than 0.0001 in, respectively.

3.2.2 ARES Rheometer

In order to test the NSS on a rotational rheometer with almost no axial compliance error, N_1 start-up measurements were made using the NSS on a stiffened ARES (Advanced Rheometric Expansion System) Scientific Rheometer (TA Instruments, Newcastle, DE) through the generosity of Professor Greg McKenna, Texas Tech University. An ARES rheometer is usually equipped with an FRT transducer as discussed in Section 2.4.2. However, in order to avoid potential errors and fragile nature of the FRT system, Professor Meckenna's group redesigned their ARES to avoid axial compliance, even transient, and equipped it with a customized Sensotec (Sensotec Inc., now Honeywell Sensotec,) semiconductor strain gage based transducer (Sensotec Model 060-G420-01) [46]. The beauty of using the semiconductor strain gage transducer is the much higher stiffness (strain sensitivity low as 0.000005 volts per microstrain) [45]. The ARES rheometer thus modified has much less axial compliance than the Weissenberg rheometer with the LVDT employed. This is true when either the strain gauge transducer or the NSS is used to measure the normal force, the latter being much more sensitive. Cone-and-plate

fixtures were used on the ARES with diameter R = 25 mm and cone angle α = 4.55 ºC (**Table 3.1**).

3.2.3 MEMS Pressure Sensor Plate

The pressure sensor plate was kindly supplied by Dr. Seong-Gi Baek, president and CEO of Rheosense, Inc. (San Ramon, CA). His company has used silicon micromachining technology [83-84] to fabricate this rheometer plate which was named the "Normal Stress Sensor" (NSS). The NSS is a monolithic rheometer plates containing miniature capacitive pressure sensors at various radical locations. Each sensor has a square pressure-sensing membrane (1 mm × 1 mm); the maximum deflection of the membrane is of order of microns (μm). This is the basis of the claim that the axial compliance of the NSS measuring system is negligible. The silicon-on-insulator (SOI) disk can easily meet the required smoothness of the rheometer plate containing pressure sensors. The SOI wafer contains three layers: a thick "handle silicon" layer that will be ultimately removed, a device silicon layer from which the membrane is fabricated, and an intermediate buried oxide layer used as an etch stop layer to allow precise control of the membrane thickness. Details of the photolithography and etching are given by Baek and Magda [44]. The result was a monolithic, perfectly smooth rheometer plate containing eight pressure sensors as sketched in **Figure 3.5**. As indicated by its name, the capacitive pressure sensor works like a capacitor that measures the voltage due to change of the gap between the silicon membrane and the conductor deposit in the silica wafer, and transferred digitally into specific reading. The baseline reading under the no pressure condition depends on the wet etching procedure and differs from each individual sensors; the output reading due to the applied external pressure is used to calculate the pressure

value using the calibration obtained using the standard pressures. The pressure sensors are symmetrically located around the plate center point at radial positions 2.5 mm, 5.0 mm, 7.5 mm and 10.0 mm, respectively. The NSS was supplied with a signal processing circuitry and DAQ software for a personal computer. The sensors were calibrated by applying known air pressure to calibration ports fabricated on the NSS. The sensor plate used on the prototype NSS Weissenberg rheometer had one of the pressure sensors at a radical position 2.5 mm from the plate center not function normally; for the NSS used with the ARES rheometer, all eight pressure-sensors were functional.

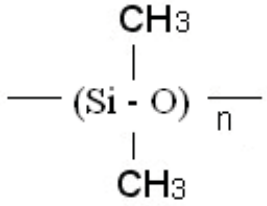

(a). Chemical formula of PDMS

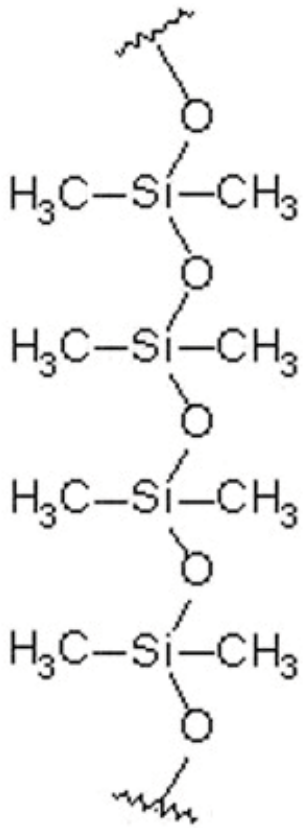

(b). Molecular structure of linear

Figure 3.1. Diagram of unit cell of linear molecule of Poly(dimethylsiloxane) (PDMS).

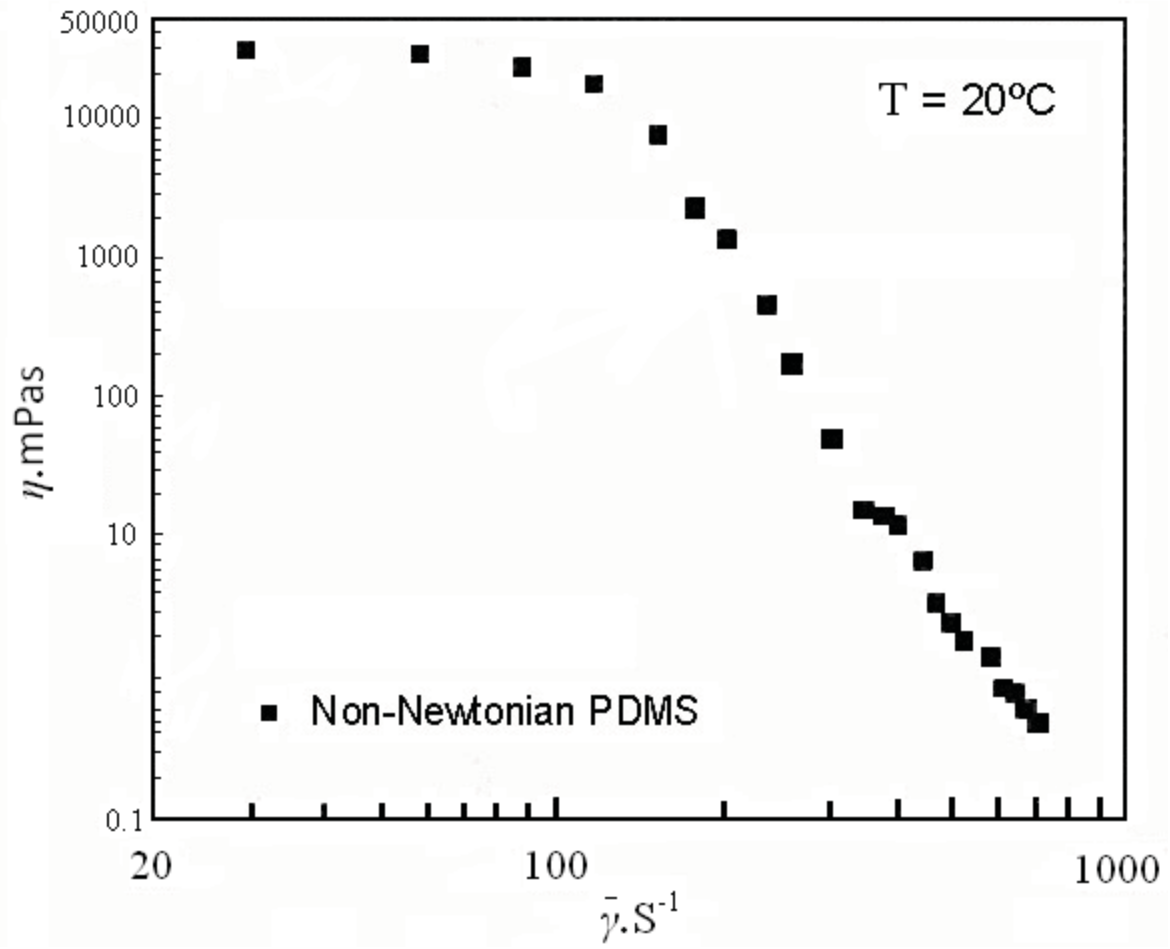

Figure 3.2. Shear thinning behavior of non-Newtonian poly(dimethyldiloxane) (PDMS) (bold square) (Adapted and simplified from Landro et al. (2003) [65])

Table 3.1. Summary of the cone-and-plate geometry

Cones #	Diameter cm	Angle °	Truncated distance μm	Sample volume ml	Rheometer adapted
1	2.5	1.13	50	0.08	Weissenberg
2	2.5	2.2	56	0.16	Weissenberg
3	2.5	4.55	50	0.1	ARES

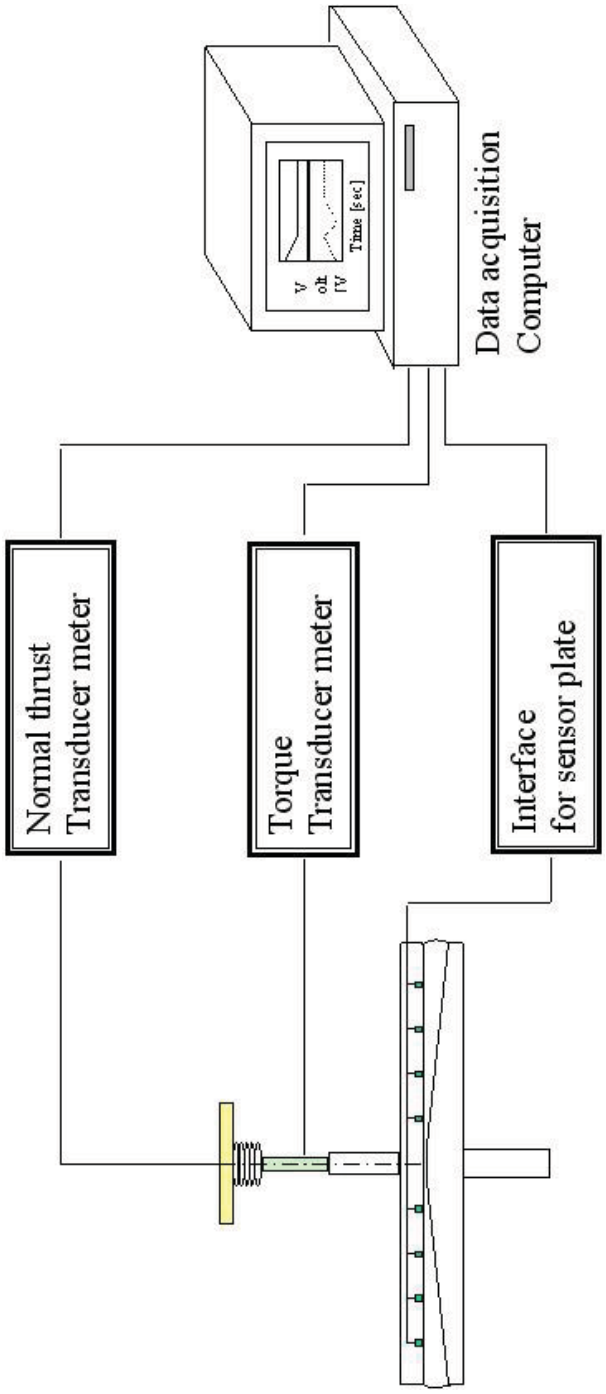

Figure 3.3. Schematic diagram of the data acquisition system with the use of LVDT and NSS.

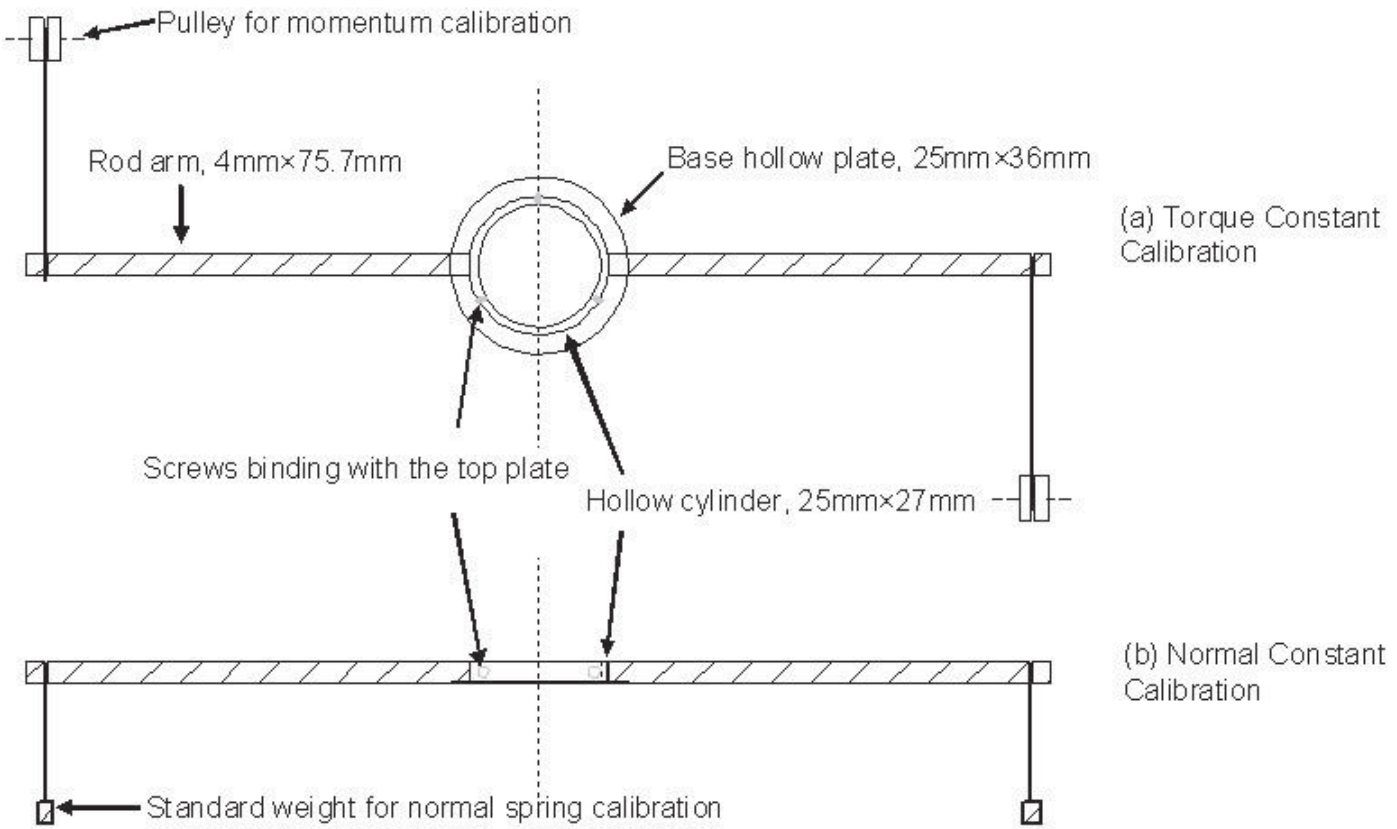

Figure 3.4. Fixture and methods of calibration: torsion bar (a) and normal spring (b).

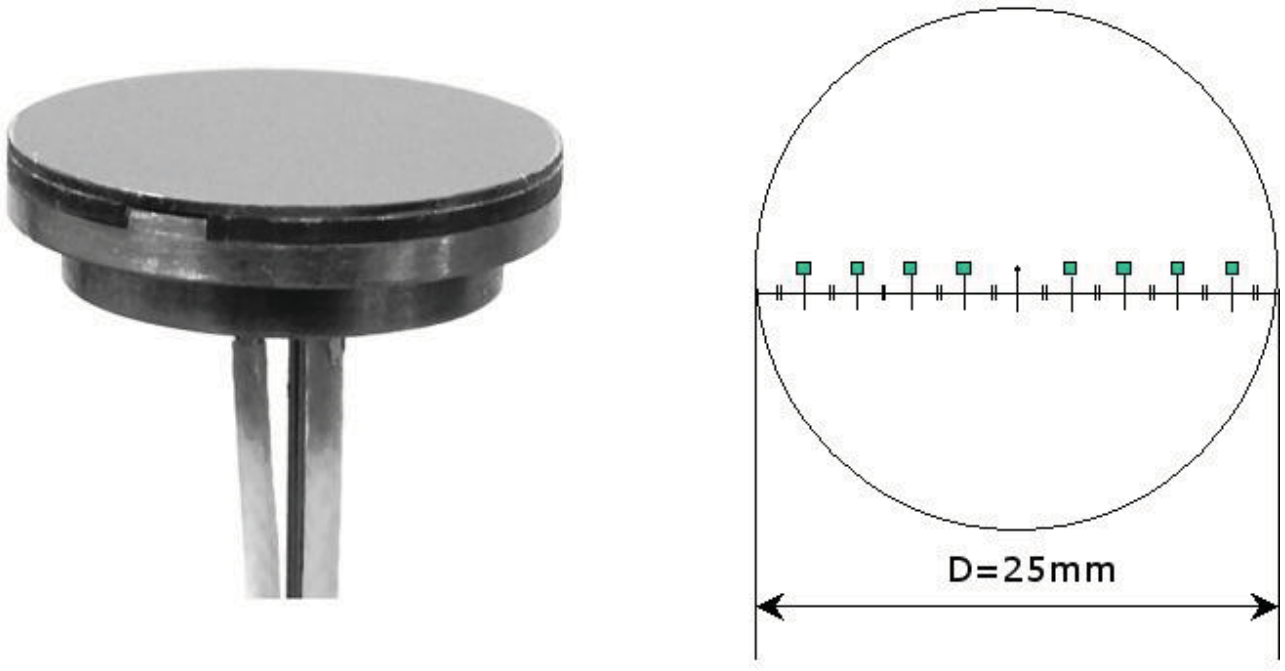

(a), the completed NSS

(b), inside view of NSS

Figure 3.5. Sketches of the NSS: (a) the completed NSS and (b) inside view of the NSS.

CHAPTER 4

RESULTS AND DISCUSSION

4.1 The Start-up Behavior of N_1 for PDMS Measurement

On start up of steady shear flow, the time t_r for N_1 to reach a steady value may be large for a viscoelastic liquid due to both the inherent material relaxation time and the axial compliance error (Section 2.3). The inherent material relaxation time λ can be estimated from steady-state properties as $\pi = \frac{\psi_{1,0}}{2\eta_0}$, where η_0 is the zero-shear-rate viscosity, and $\psi_{1,0}$ is the zero-shear-rate limit of the first normal stress difference coefficient [19]. **Figure 4.1** and **Figure 4.2** show the steady state values of η and N_1, as measured for the PDMS sample on the Weissenberg rheometer using the LVDT measuring systems, with 25 mm plate and 0.04 rad cone. The measured η_0 values are shown in **Table 4.1**, obviously 294 ± 8 Pa·S, as expected from the supplier's values. Using the low-shear-rate values of N_1 in **Figure 4.2**, $\psi_{1,0}$ is estimated as 0.9 Pa, giving $\lambda \approx 0.05$ s. **Figure 4.3** shows the start-up and flow cessation behavior of N_1 for the same PDMS material on the Weissenberg and the response time t_r far exceeds λ ($t_r \approx 15$ s). Here t_r is defined as time required for N_1 to decay to 37% of its steady-state value after

flow cessation. This demonstrates that the axial compliance error is substantial, probably due to high sample viscosity and the highly sensitive normal force spring on the Weissenberg rheometer ($\lambda = \frac{\Psi_{1,0}}{2 \cdot \eta}$). The ARES rheometer modified to reduce axial compliance (Section 3.4) was used to obtain N_1 start-up results for NIST fluid SRM-1490 using the NSS pressure sensor plate (unfortunately PDMS was not available). Values for η_0 and N_1 supplied by NIST for SRM-1490 (**Table 4.1**) can be used to estimate the relaxation time of SRM-1490 ($\lambda \approx 1s$). **Figure 4.4** shows the start-up and flow cessation behavior of N_1 for SRM-1490 fluid in the modified cone-and-plate ARES, with 0.08 rad cone and plate of 25 mm in diameter, under the shear rates of 20 s^{-1}. The relaxation curve is used to estimate the response time of SRM-1490, $t_r \approx 1.27 \pm 0.3$ s. This is quite close to the inherent relaxation time of the SRM-1490 relaxation time, $\lambda \approx 1$ s. The measured N_1 response time, t_r, and inherent relaxation time, λ, of PDMS fluid and NIST SRM 1490 are summarized in **Table 4.1**.

The measured N_1 response time, t_r, is expected to be equivalent to the theoretical calculated relaxation time λ in the absence of any measurement error. However, as shown in **Table 4.1**, the t_r value of PDMS fluid greatly exceeds λ; whereas $t_r \approx \lambda$ for NIST SRM-1490 fluid.

The difference in these results for these two fluids is considered to be due to the two different measuring instruments: the Wenssenberg R17 rheometer with a large axial compliance and the modified ARES with little axial compliance. The results reveal the dramatically delayed response of normal force measurement on the R-17 rheometer due

to the instrument compliance. Axial instrument compliance may lead to a misleading transient response measurement giving unreliable estimations of the material characteristic relaxation time measurement. The results also show that this problem can be avoided by using NSS to measure the transient N_1 response on a stiff rheometer.

4.1.1 Effect of the Natural Frequency of the Measuring System

Figure 4.5 shows the start-up behavior of the apparent N_1 value of PDMS fluid measured in the Weissenberg Rheogoniometer, with 0.038 rad cone and plate of 25 mm diameter, at the shear rate of 9.8 s^{-1}. The time-dependent curves shown in **Figure 4.5** were obtained simultaneously by two normal force measuring systems: the LVDT system (open circles) and the NSS system (stars). The LVDT provides an analog signal whereas the NSS provides the pressure value at the locations of the eight sensors every 0.1 s. These local pressure readings were time-average over an interval of 1 second, and the result was fit to Equation 2.25 for the radical pressure profile in order to calculate N_1. Superficially, the LVDT curve is smoother, but this is only because the LVDT cannot detect higher frequency normal force variations. In the Weissenberg rheometer under the conditions of **Figure 4.5**, the period of cone rotation is 16.7 s. This is almost exactly equal to the period of oscillations of the highly regular N_1 curve measured by the NSS. **Figure 4.5** reveals that each of these two measuring system has its own natural frequency: the natural frequency of the NSS is high as 137 kHz as reported by the Rheosense Inc. to be, while the natural frequency of LVDT system is apparently too low to detect the fluctuations of the normal force signal of high frequency associated with imperfections in the motor rotation. As a result, the measurement of the LVDT gives a fault impression that the flow field is very uniform and stable. In this manner, the NSS

with a high natural frequency is more reliable than the traditional LVDT system in detecting high frequency material response.

4.1.2 Effect of the Tilted Misalignment of Cone and Plate on the Radical Pressure Profile

As discussed in Section 2.3, the typical degree of tilted misalignment may cause radical asymmetry in the local pressure distribution and a shift of the maximum local pressure position, and the errors may be annihilated by the "averaging effect". **Figure 4.6** shows the local time-averaged pressures of the PDMS fluid as measured by the pressure sensors located in different positions of the NSS under shear rate of 9.8 s^{-1} with the use of 0.038 rad (2.2°) cone on the Weissenberg rheometer. Prior to measurement, the alignment of the cone and plate was adjusted following rheometer manual specifications (Chapter 3). The pressure data are shown in **Figure 4.6**, and the origin point 0 of the abscissa represents the center of the plate; the negative and the positive abscissa of the coordinates represent the left and the right side of the pressure sensor plate, respectively; and values of 5, 7.5, 10 represent the distances of the pressure sensors in mm from the centre of the plate. Only six pressure sensors are located 2.5mm from the plate center. On both sides of the pressure sensor plate, the pressure sensors closest to the center of the plates measured the higher local pressures, as expected from Equation 2.25 when $N_1 + 2N_2$ being positive. Due to the second type of tilted misalignment (**Figure 2.7**), the local pressures measured on the left side and the right side were not equivalent in magnitudes, for either clockwise or counter clockwise rotation directions. However, as shown in **Figure 4.6**, the local pressures measured on the left hand side of the plate for the clockwise rotation were very close to those measured on the right side of the plate for

counter clockwise rotation, and vice versa. Thus the pressure error due to misalignment can be removed by averaged over both sides of plate for a given rotation direction, or by averaging the pressure on one side of the plate over both rotation directions. These observations agree with Adam's results (**Figure 2.9**), thus confirming that the pressure distribution for Newton liquids applies to the non-Newtonian liquids. According to the simulation results of Wedgwood's group for the shear-thinning materials (Chapter 2), the maximum slope of the tilt is between line of 0 to π and line of $\frac{\pi}{2}$ to $\frac{3\pi}{2}$ in the top view coordinates as shown in **Figure 4.6**. The exact maximum tilted line can be located if the phase shift of the material can be determined. However, this calculation will be defeated to the future works.

4.1.3 Effect of 'Wobble' on the Time-dependent Local Pressure

In addition, a new phenomenon termed the "wobble error" was discovered based on the observations shown in **Figure 4.7**. **Figure 4.7** contains the output signals of pressure sensors at the same distance from the center of the plate but on the opposite sides. Both signals oscillate with a period equal to the period of cone rotation, but the oscillations are 180 degrees out of phase. The "wobble error" may be caused by the third type of misalignment (see **Figure 2.7 (c)**). The measurements suggest that the misalignment in our Weissenberg R-17 has a combination of the tiled plate and tiled cone with a perpendicular rotating axial, as sketched in **Figure 4.8**. However, the newly discovered Wobble error has not yet been systematically investigated. It is interesting to note that similar effect is observed with the NSS for cone-plate flows of NIST SRM-2490

on an ARES rheometer (University of Minnesota), suggesting this is a universal phenomenon in measuring the N_2 using the pressure distribution method.

4.2 Steady-shear Flow Properties of Solvent-free Ambiance Temperature PDMS

Despite of the flow irregularities on the Weissenberg rheometer just discussed, with appropriate averaging, it was found to be possible to use the NSS to measure the shear properties, i.e. the first and the second normal stress differences and the viscosity of the shear pure PDMS melt at room temperature.

4.2.1 Measurement of the Radial Local Normal Pressure Profile

Figure 4.9 shows the time-averaged radial pressure profile, and the misalignment error leading to radical asymmetry is apparent. However, as discussed in Section 4.1, this error can be eliminated by averaging local pressure over both sides of the plate and/or over both clockwise and counterclockwise rotations. **Figure 4.9** shows the results so obtained at various shear rates. **Figure 4.9** contains the local pressure function of the normalized position, $\frac{r}{R}$, where r is the position of the pressure sensor and R is the radium of the pressure sensor plate. Equation 2.25 shows that theoretically the local normal pressures (Π_{22}-P_0) is a linear function of logarithm of the normalized position, $\ln\left(\frac{r}{R}\right)$. As discussed in Section 2.4.2.1, N_1 and N_2 can be obtained from the slope and intercept of this linear function. **Figure 4.9** shows the plots of the measured local normal pressure against the normalized radial position under a series of shear rates: 6.19 s^{-1}, 7.80 s^{-1}, 9.82 s^{-1}, 12.38 s^{-1} and 15.6 s^{-1}. It was observed that the PDMS sample could be

sheared up to the maximum shear rate of 15.6 s^{-1} before it exhibited edge fracture. The local pressures plotted shown in **Figure 4.9** were averaged in three manners: with respect to time, clockwise and counterclockwise rotations, and left hand and right hand sides of the pressure plate. In this way the misalignment error can be eliminated as proved in Section 4.1. It should be noted that, while time-averaging is obviously valid in the steady state; for the second and the third manners of averaging, an assumption has been made about the average effects on the wedge flow as discussed in Section 2.2. This assumption is justified by the closeness of the experimental radial pressure profiles in **Figure 4.9** such that expected for an ideal cone-and-plate flow.

As shown in **Figure 4.9**, all the averaged pressure distribution functions are linear functions of the logarithm of the dimensionless position. The effects of the shear rate are also demonstrated: the intercept of linear function of the pressure distribution increases with the increasing shear rate; the slope of the local normal pressure function is negative and decreases in magnitude with the decreasing shear rates. As discussed in Chapter 2, the linear pressure distribution function can be used to determine the properties, N_1 and N_2, of the test fluid. According to Equation 2.25, N_1 and N_2 are both parameters of the pressure distribution function, in which the intercept represents the negative value of N_2 and the slope indicates the term including N_1 and N_2, that is, -(N_1+2 N_2). The values of N_1 determined from the averaged pressure distributions in **Figure 4.9** are compared to the values of N_1 independently measured with the normal force LVDT in **Figure 4.10**. The agreement is excellent, confirming once again that the averaging procedure

eliminates the effects of flow irregularities of flow irregularities. Values of the ratio $\psi = -\frac{N_2}{N_1}$ obtained from **Figure 4.9** are compared to literature results in the next section.

4.2.2 Determination of the Normal Stress Ratio, $\psi = -\frac{N_2}{N_1}$, of Solvent-free PDMS at Room Temperature

The normal stress ratio, $\psi = -\frac{N_2}{N_1}$, is a frequently reported elastic property (**Table 2.1**) just because it is almost independent of shear rate and its value correlated with the flow instability of materials. **Figure 4.11** shows the measured normal stress difference ratio of pure PDMS melt at room temperature obtained from the averaged pressure profiles of **Figure 4.9** to facilitate comparison with previously published results for polystyrene [69]. The abscissa is the dimensionless shear rate ϖ_i, defined as $\varpi_i = \frac{\dot{\gamma} \psi_{1,0}}{2\eta}$. The measured average value of the normal stress ratio for PDMS fluid was 0.14 ± 0.01. The normal stress ratio reported here is within the range of ψ values (0.101—0.154) measured by Di Landro *et al.* (2003) [65] for non-Newtonian PDMS melts (Aldrich PDMS 100 and Polymerland PDMS 600) at 20 °C using the rod-climbing method.

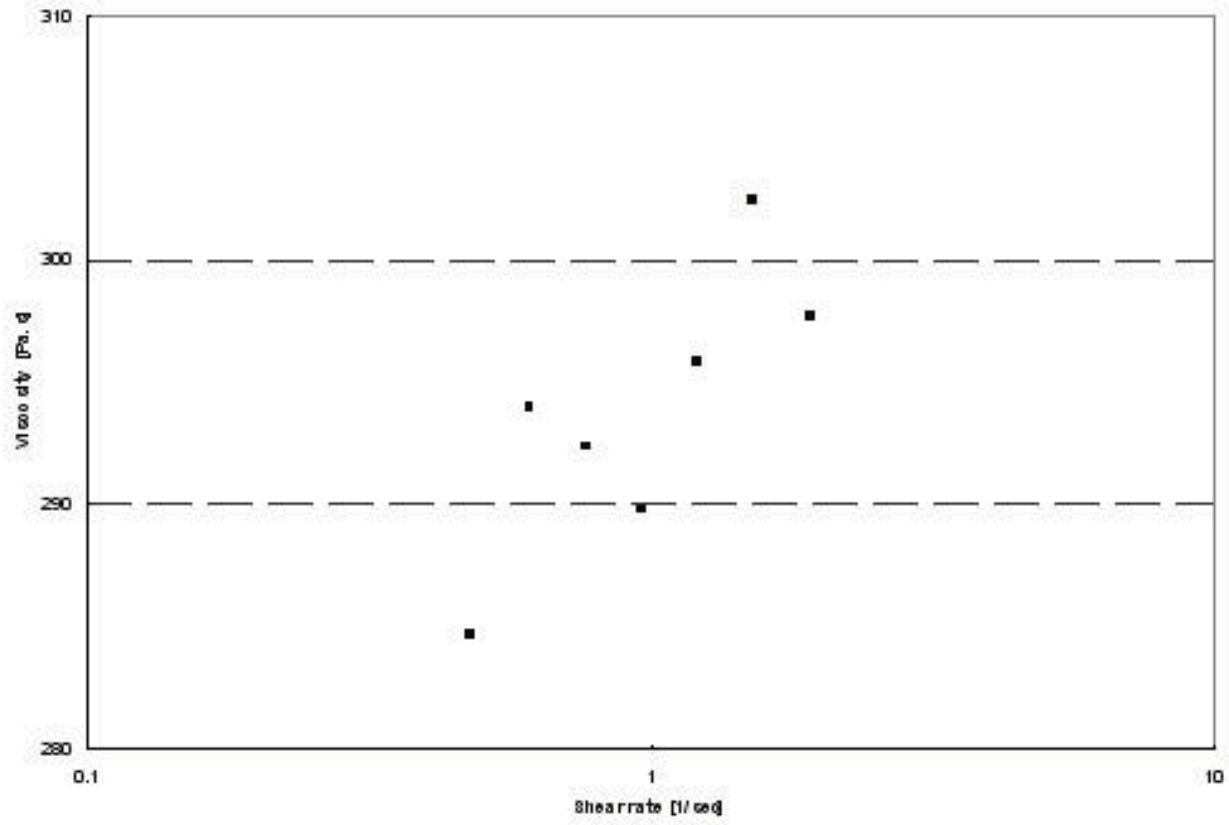

Figure 4.1. Viscosity of Rheodosil PDMS vs. shear rate measured in cone-plate Weissenberg R-17 rheometer at 25 ^{o}C. Cone angle was 0.038 rad, cone radius was 12.5 mm.

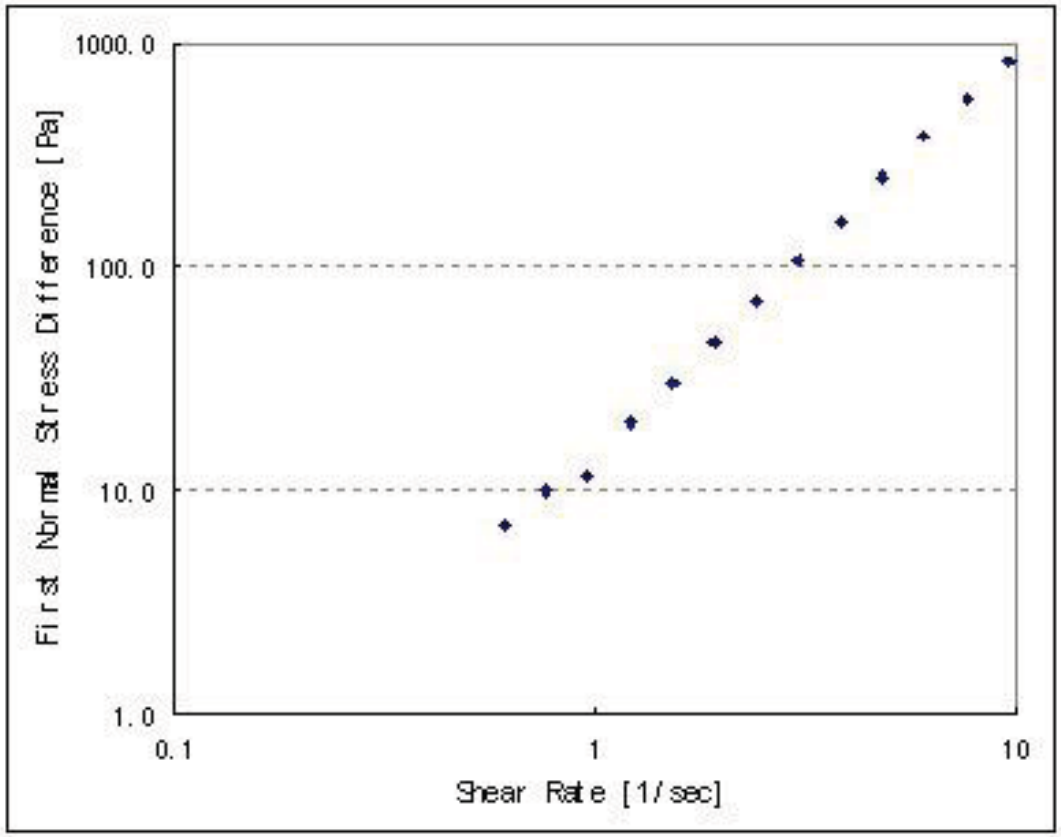

Figure 4.2. Steady-state N_1 shear rate as measured for PDMS sample at room temperature using the LVDT on Weissenberg R17 rheometer. Cone angle was 0.038 rad, cone radius was 12.5 mm.

Table 4.1. Material relaxation time vs. observed response time.

	NIST SRM-1490 on ARES						PDMS on Weissenberg
	1 (CCW)	2 (CCW)	3 (CW)	4 (CW)	Avg.	SD	
Measured relaxation time of NIST Fluid, s	1.057	1.100	1.067	1.079	1.076	0.018	15.28
Averaged N_1, Pascal	554.9	537.3	521.0	525.7	534.7	15.1	2504.5
Theoretical estimated relaxation time, s	1.047						0.05

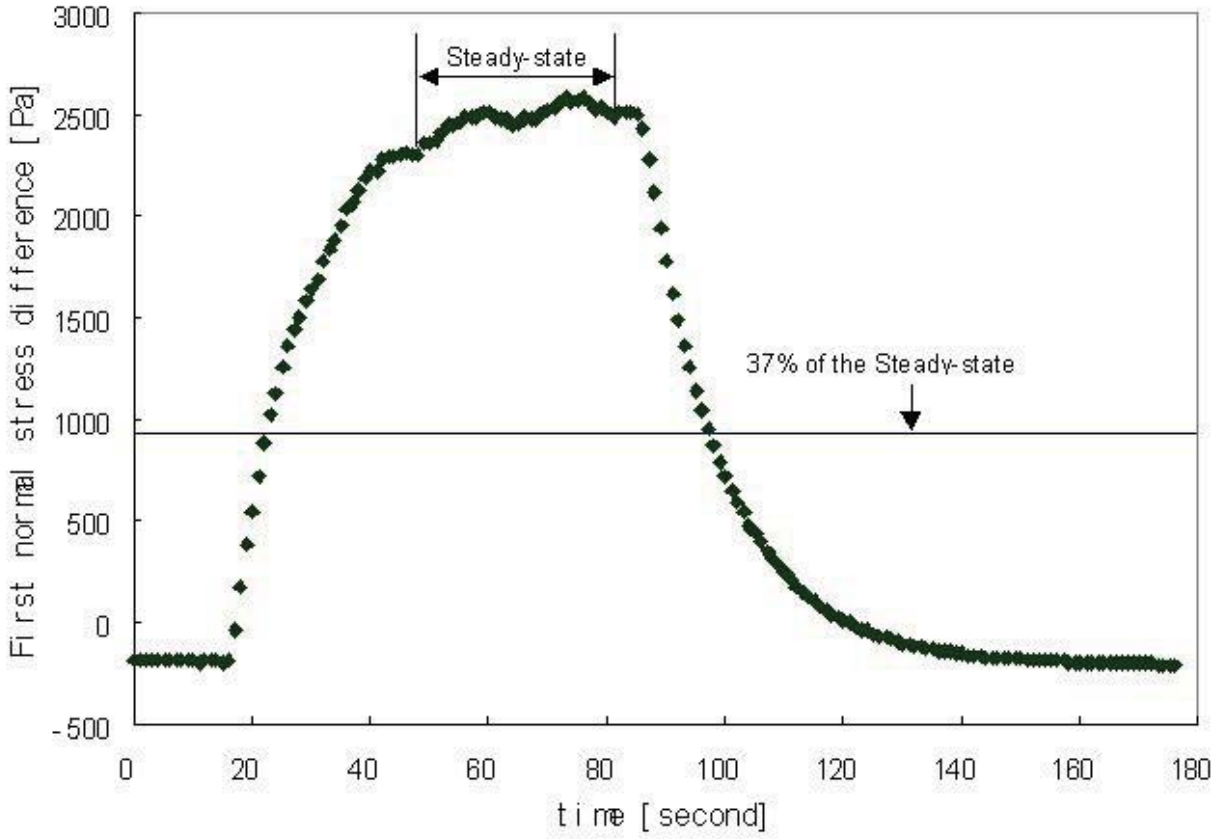

Figure 4.3. Start-up and ralxation behavior of the appearent N_1 value, as measured at shear rate 9.8 s^{-1} for PDMS sample using the LVDT in a cone-plate flow on the Weissenberg R-17 rheometer at ambient tempreture (25±1 ^{o}C). Cone angle was 0.038 rad, cone radius was 12.5 mm. Shear flow was started at time equal 15 s and halted at 85 s.

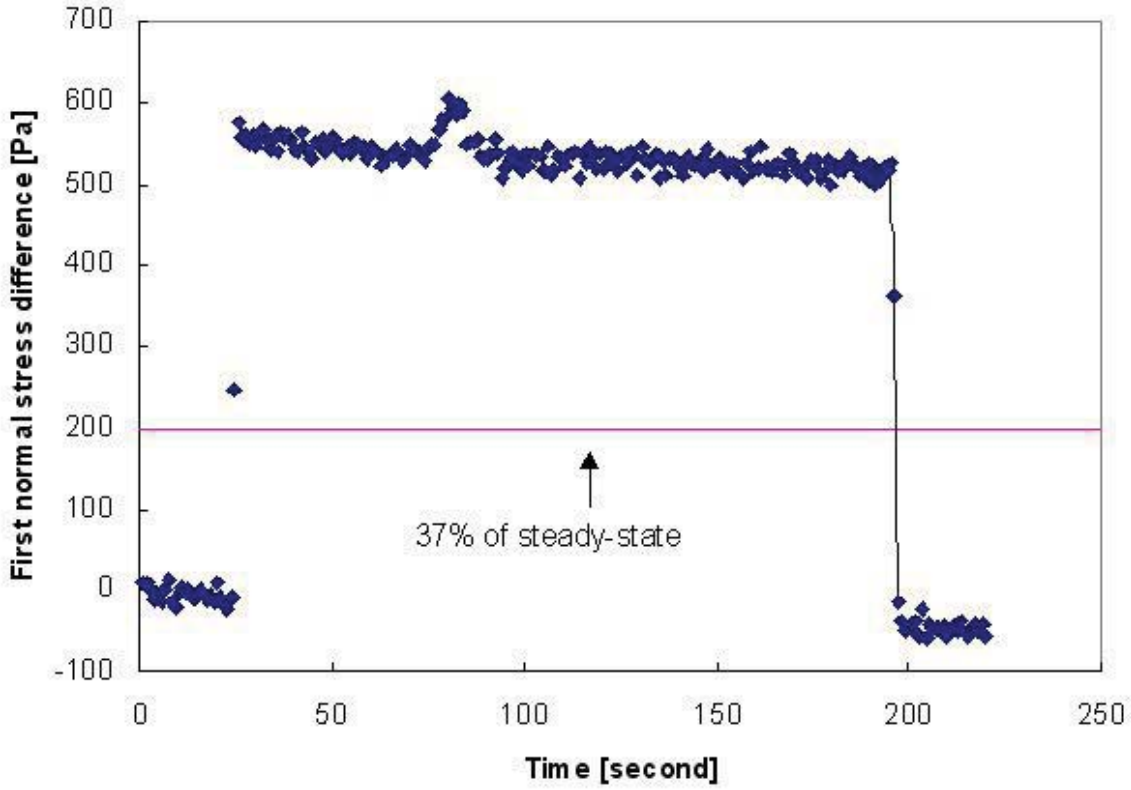

Figure 4.4. Start-up and relaxation behavior of the apperent N_1 value, as measured at shear rate for a standard polyers solution (NIST SRM 1490) using the pressure sensor plate in a cone-plate flow on ARES rheometer modified to reduce axial compliance at 25 ^{o}C. Cone angle was 0.079 rad, cone radius was 12.5 mm. Shear flow was started at time equal 25 s and halted at 200 s.

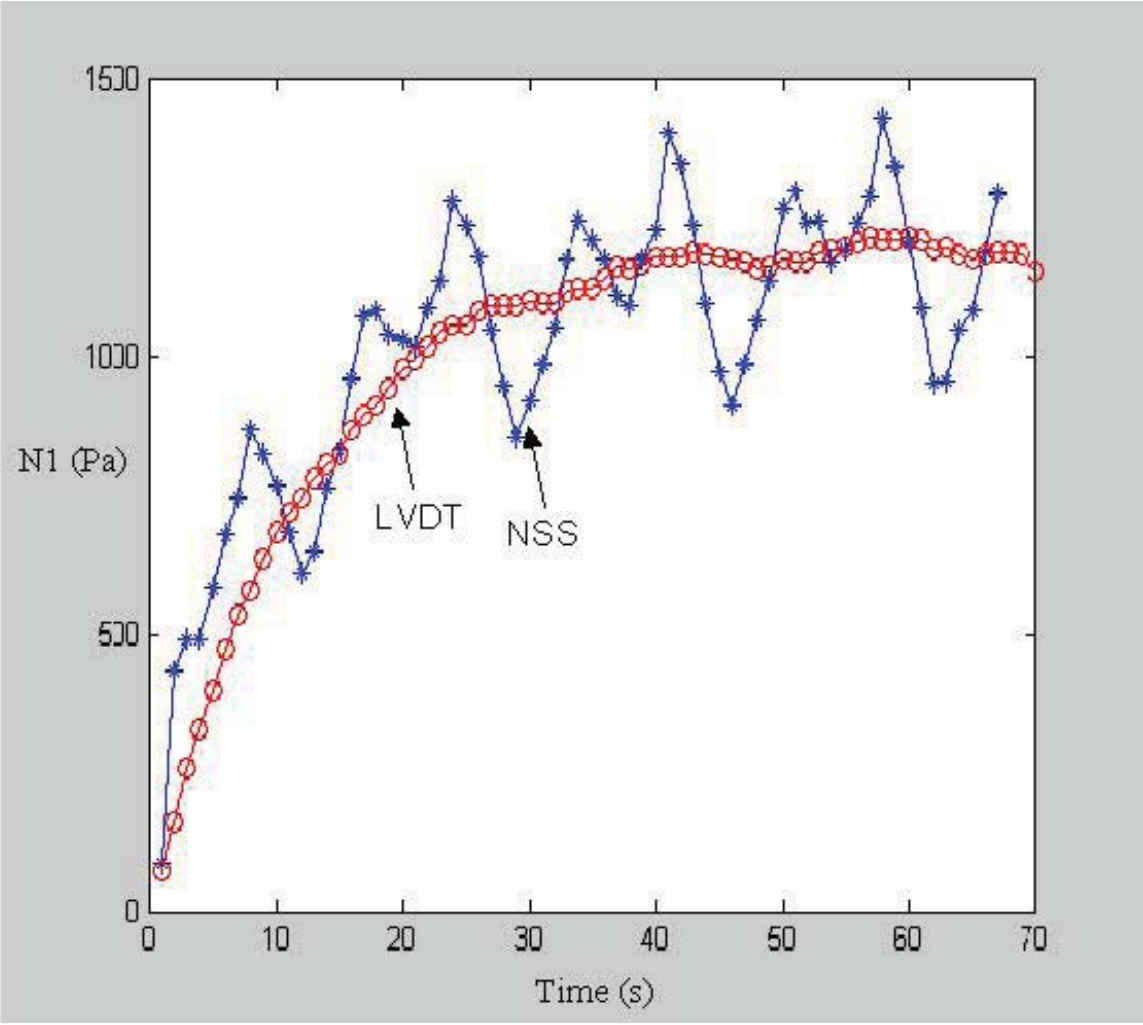

Figure 4.5. Time-dependent apparent N_1 value after start-up of flow at shear rate 9.8 s^{-1} for PDMS sample in Weissenberg R-17 rheometer as measured simultaneously with two different normal force systems at 25 ^{o}C: (o) LVDT; (*) pressure sensor plate. Cone angle was 0.038 rad, cone radius was 12.5 mm.

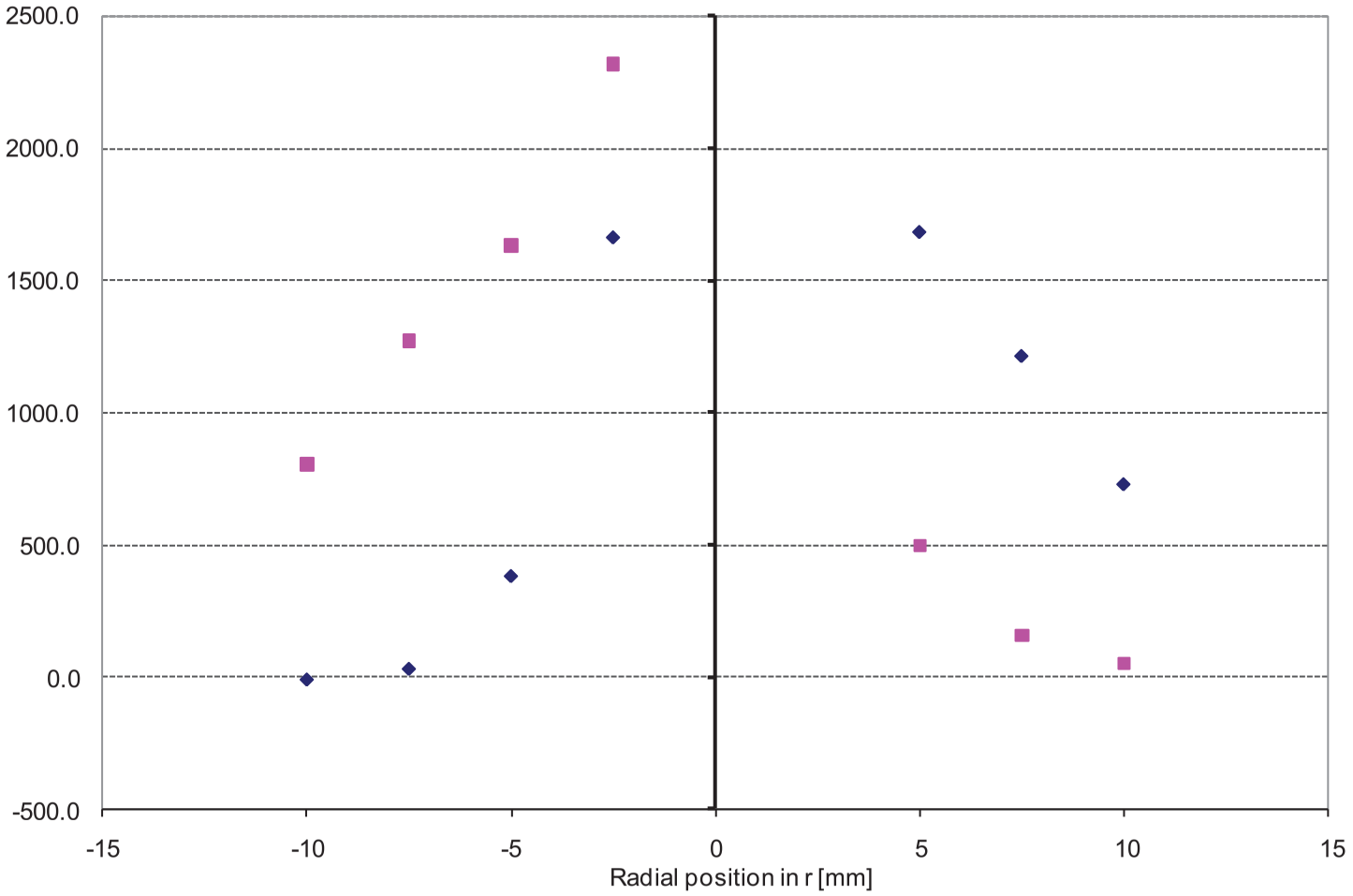

Figure 4.6: Comparison of time averaged local pressure measured on opposite sides of the pressure sensor plate during steady shear flow of PDMS on the Weissenberg rheometer at 9.8 s^{-1} at 25 ^{o}C. Results for both clockwise (square symbols) and counterclockwise cone rotations are shown. Values on the abscissa give the distance from the plate center point, with opposite signs corresponding to opposite halves of the pressure sensor plate. Cone angle was 0.038 rad, cone radius was 12.5 mm.

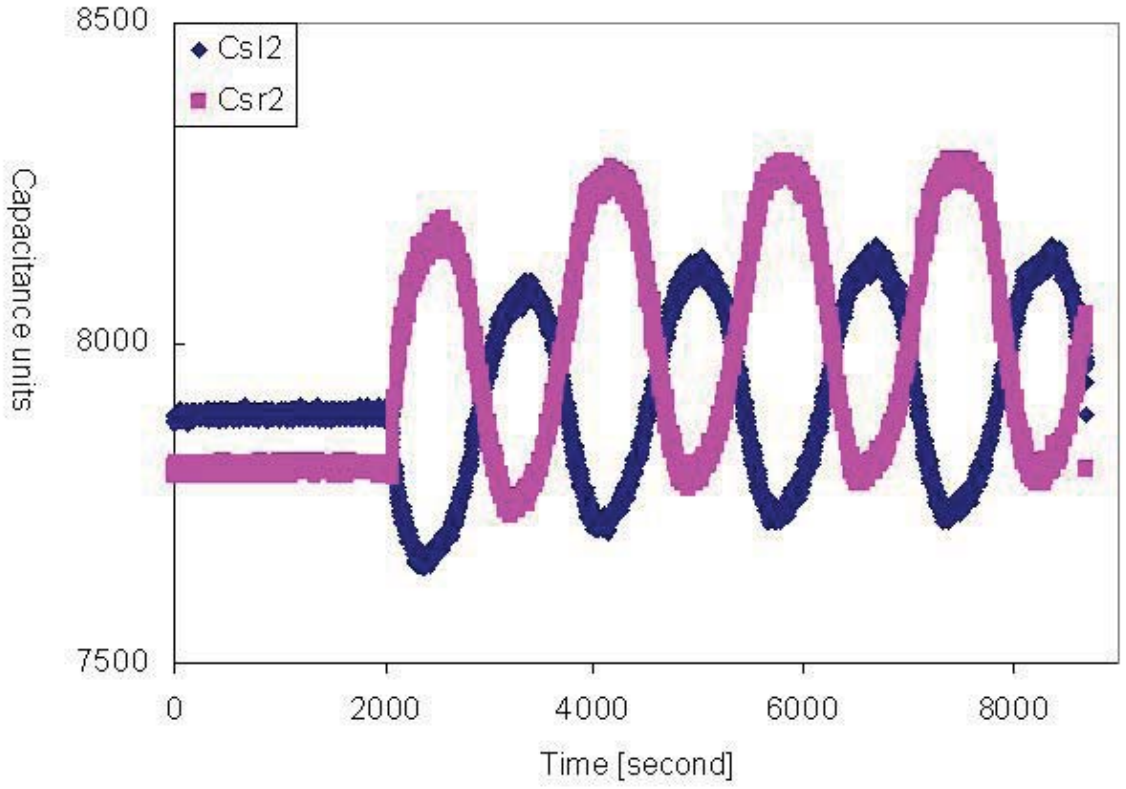

Figure 4.7. Comparison of time-dependent signals measured by local pressure sensors on opposite sides of the plate during steady shear flow of PDMS on the Weissenberg rheometer at 9.8 s^{-1}. Both sensors are 5.0 mm from the center point of the plate. Cone angle was 0.038 rad, cone radius was 12.5 mm.

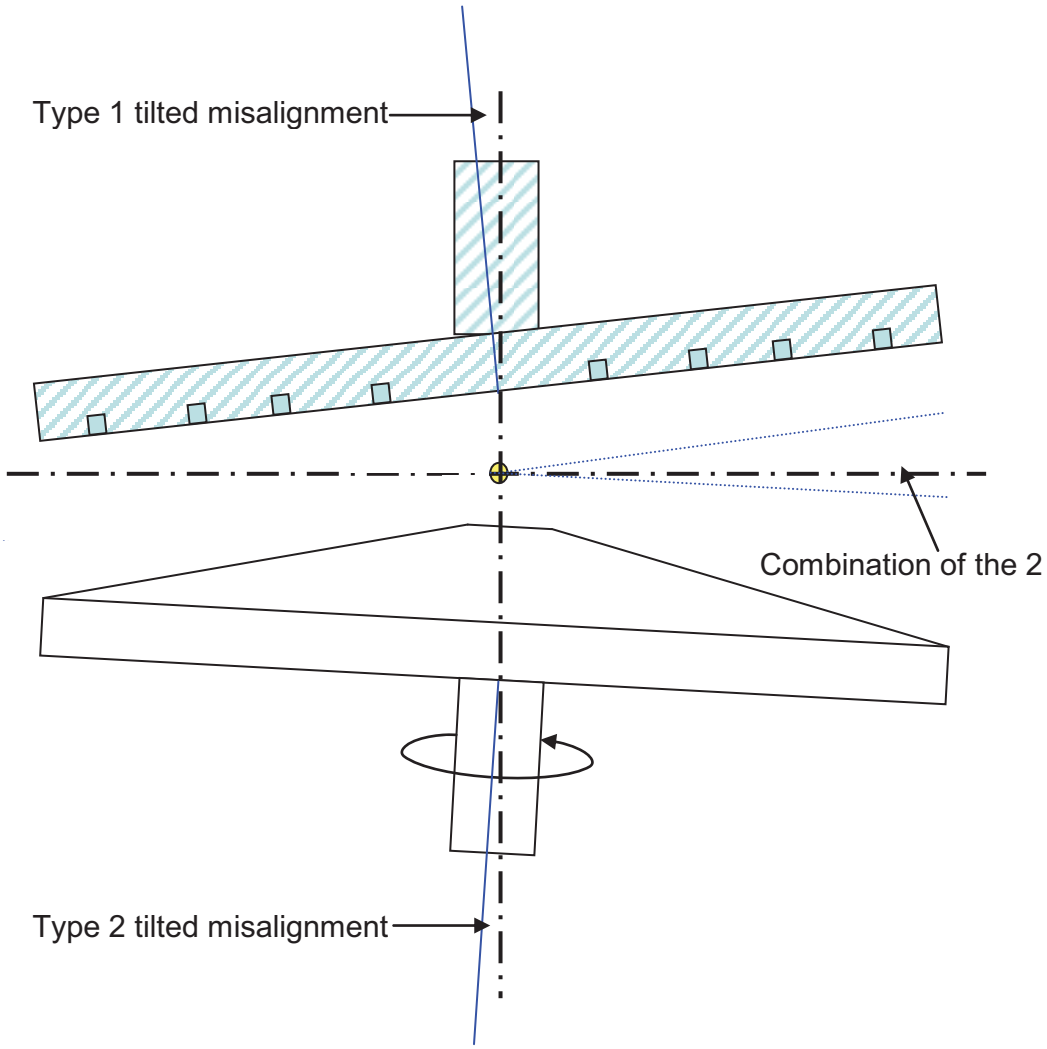

Figure 4.8. The Combination of the two types of flatness misalignment.

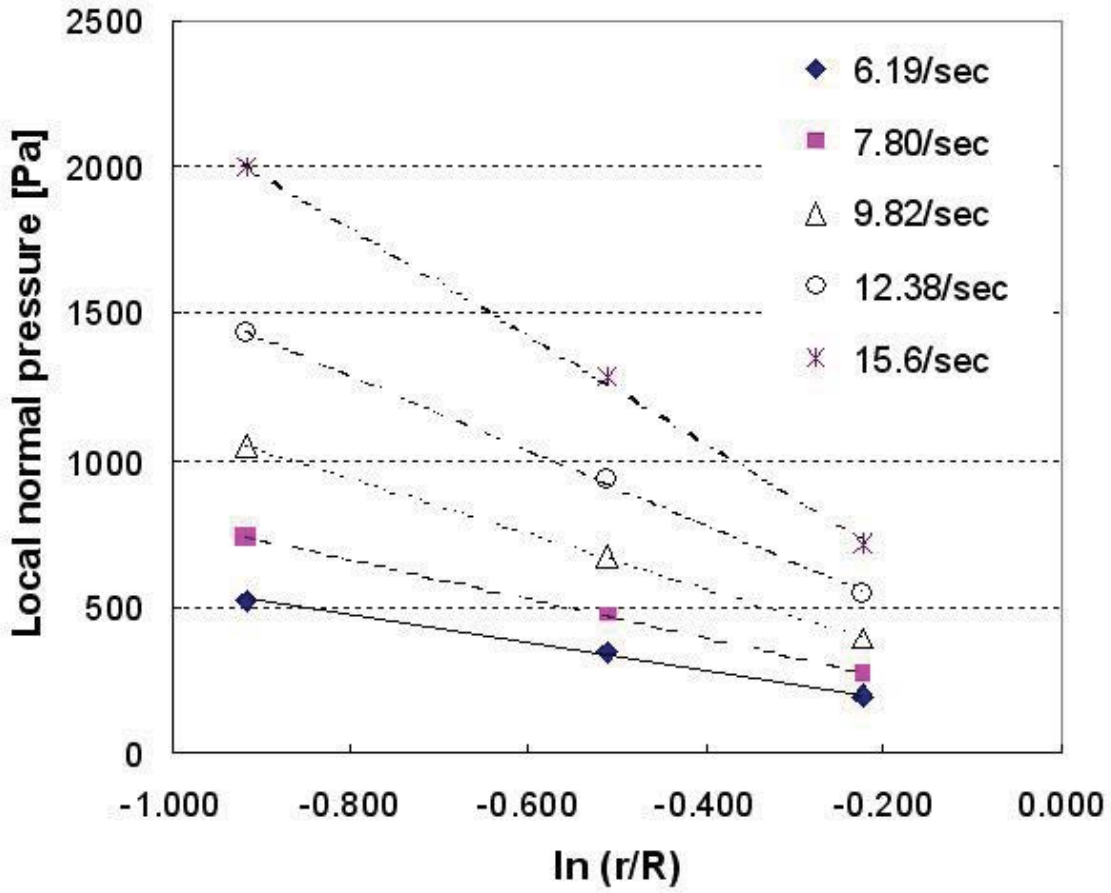

Figure 4.9. Plots of local normal pressure as a function of ln(r/R) at the shear rates shown in the legend, as measured for PDMS using NSS on Weissenberg rheometer of room temperature. Cone angle was 0.038 rad, cone radius was 12.5 mm, and local pressures have been averaged over both halves of the NSS and over both clockwise and counterclockwise rotations.

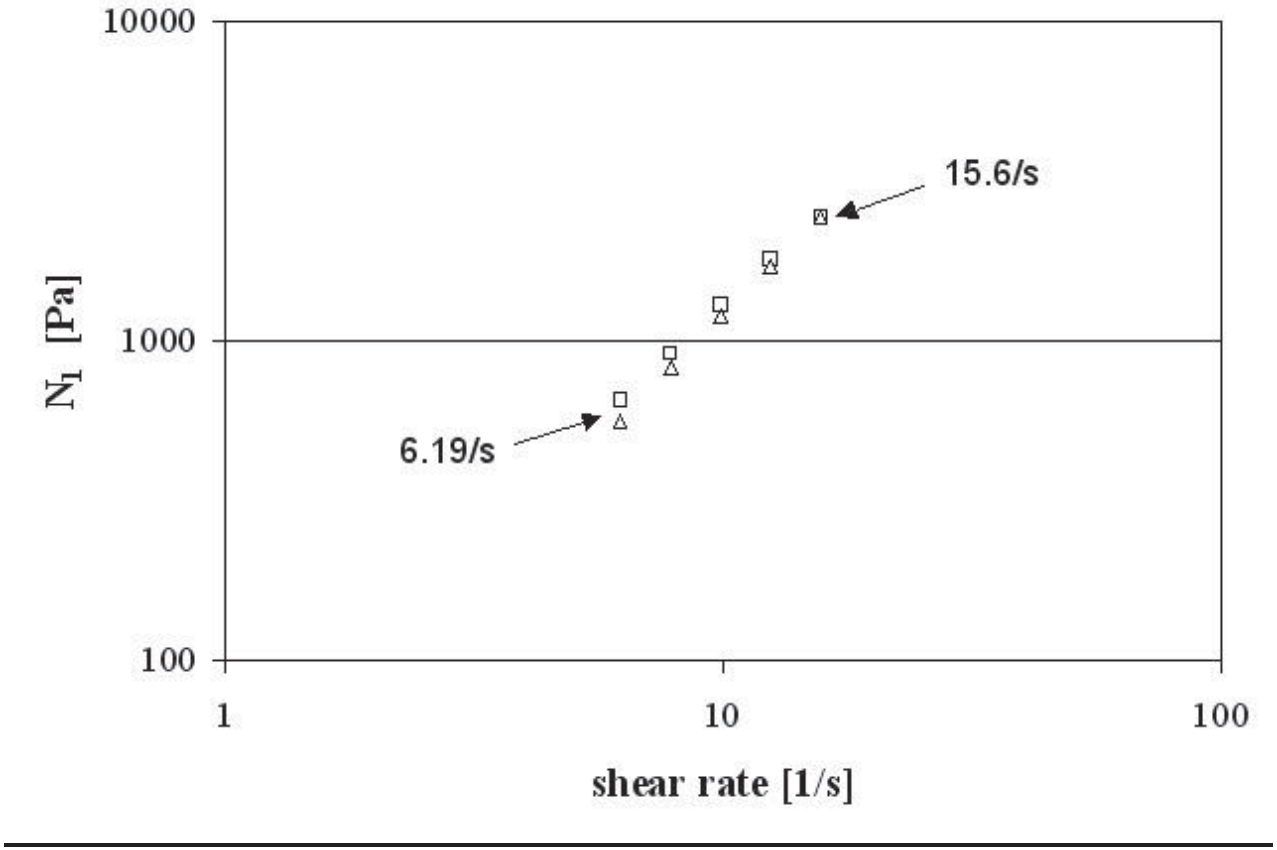

Figure 4.10. Comparison of N_1 values obtained by two independent methods: from NSS pressure profiles of **Figure 4.9** (square) and from LVDT (triangle).

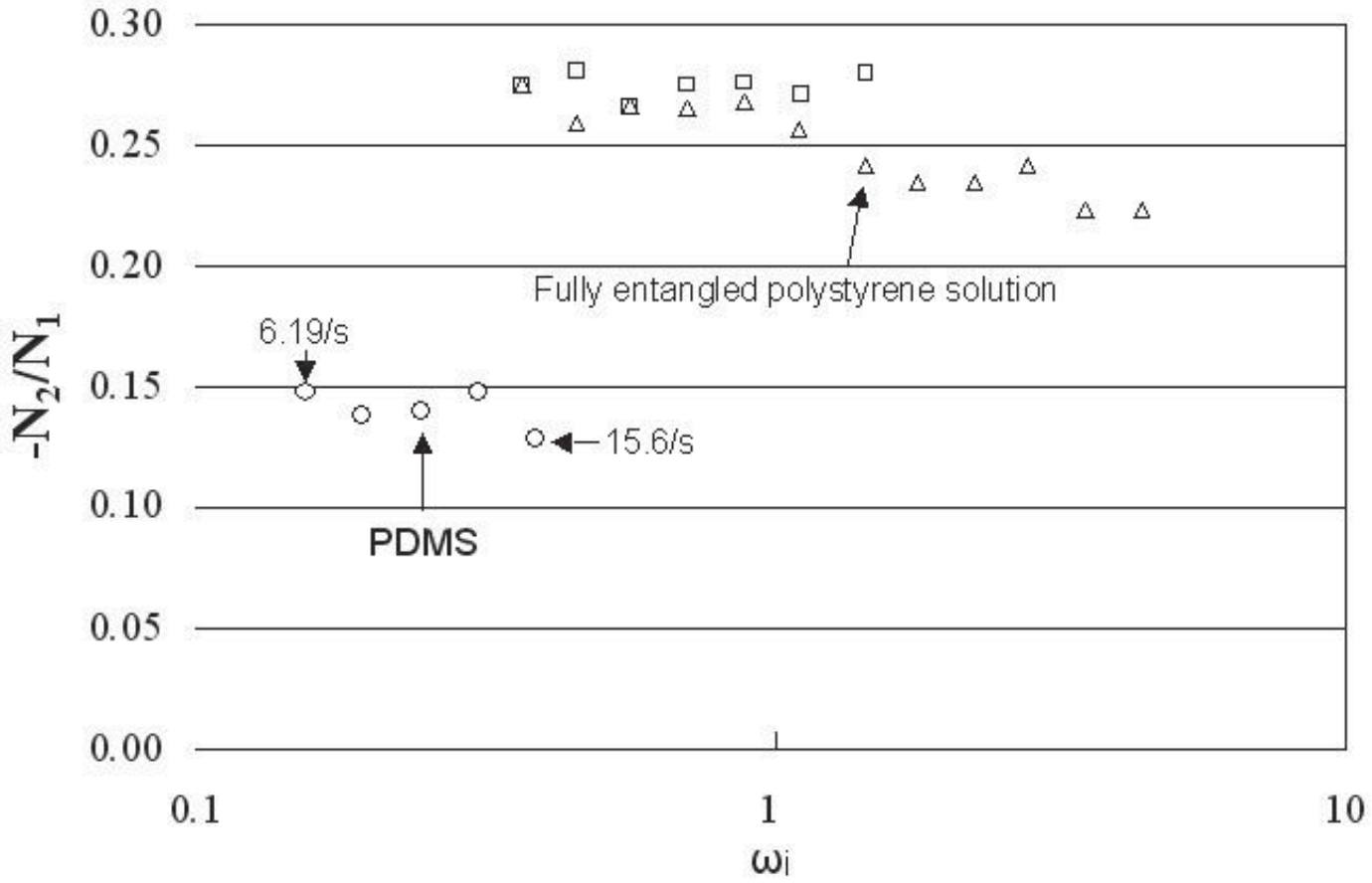

Figure 4.11. Dimensionless Weissenberg number as obtained using radial pressure distribution method for polystyrene solutions (Reference [69]), and PDMS (this thesis).

CHAPTER 5

CONCLUSIONS

This work focused on the application of a novel MEMS pressure sensor plate with the traditional rotating rheometer to evaluate various error sources, such as misalignment of the cone and the plate, and the effects of axial compliance and natural frequency. It also focuses on the measurement of the normal rheological functions of a viscoelastic material. Comparison was made when possible to normal force measurements made with a traditional LVDT/normal force spring system. A sensitive spring must be used with the LVDT system, which results in a relatively large axial compliance and relatively low natural frequency.

The transient apparent first normal stress N_1 value upon startup shear flow obtained with the NFS-LVDT and the NSS showed the effects of the natural frequency of the measuring system. The LVDT system has a low natural frequency; hence it cannot follow the relatively high frequency of the signals associated with motor vibrations. Thus, it cannot distinguish between flow is highly smooth and stable and high frequency disable. By contrast, with a much higher natural frequency, the NSS is able to detect the signal periodic fluctuations associated with the rotations of the rheometer motor. Axial compliance may affect the response of the rheometer for the apparent N_1 value upon start-up of shear flow. If axial compliance is negligible, then this response time can be used to estimate the average relaxation time of the material. This was found to be the case

for the N_1 startup nehavior of NIST fluid SRM-1490 measured with the NSS on an ARES theometer modified to increase axial stiffness. This was not the case for LVDT measurements of PDMS transient behavior on the Weissenberg rheometer. That is, the response time observed for the apparent N_1 value upon startup of shear flow for PDMS greatly exceeded the average relaxation time calculated from the steady shear properties.

Local pressure measurements made with the NSS were used to study the misalignment effect. The results show that with a typical degree of misalignment, in the cone-and-plate geometry, the local pressures are not symmetric about the center point of the rheometer plate due to the "Wedge effect" first noted by Adams and Lodge [32]. However, the misalignment error of the local pressure value is aqntisymmetric about the plate center point, and thus can be eliminated by averaging the pressure profile over both sides of the rheometer plate, at least for PDMS. It can also be eliminated by averaging over both clockwise and ccouterclockwise rotation results. This conclusion agrees with the simulation prediction by Wedgewood's group [33].

The pressure profiles so averaged agree with fluid mechanics predictions for ideal cone-and-plate and were used to calculate N_1 and N_2 fro PDMS, and the normal stress ratio $\psi = -\frac{N_2}{N_1}$. The value obtained for $-N_2/N_1$ was relatively insensitive to shear rate and equal to 0.14 ± 0.01. This is reasonably close to the values reported by Di Landro *et al.* [65], $-N_2/N_1$ = 0.105-0.189, as measured for PDMS samples of various molecular weights using the rod-climbing method. Lastly, a periodic oscillation in the measured local pressure value during steady shear flow of unknown origin was observed. The

period of the oscillation equaled that differed by 180 degrees on the opposite sides of the rheometer plate.

REFERENCES

1. J. M. Dealy, "Rheometers for Molten Plastics", Van Nostrand Reinhold Press: **1982**

2. K. Walters, "Rheometry: Industrial Applications. Materials Science Research Studies Series, Volume 1", John Wiley and Sons Ltd Press: **1980**

3. Chang Dae han, "Rheology in industry Processing", Acadamic Press: **1976**

4. R. G. Larson, At&T Bell Laboratories, "Review: Instabiliteis in Viscoelastic Flows", *Rheol. Acta* **1992**, *31*, 213

5. J.-M. Piau, N. E. Kissi, B. Tremblay, "Influence of Upstream Instabilities and Wall Slip on Melt Fracture and Sharkskin Phenomena During Silicones Extrusion Through Orifice Dies", *J. Non-Newtonian Fluid Mech.* **1990**, *34*, 145

6. S. Nigen, N. E. Kissi, J.-M. Piau, S. Sadum, "Velocity Field for Polymer Melts Extrudion Using Partical Imagine Velocitmery Stable and Unstable Flow Regimes", *J. Non-Newtonian Fluid Mech.* **2003**, *112*, 177

7. K. Chen, "Interfacial Instability Due to Elastic Stratification in Concentric Coextrusion of Two Viscoelastic Fluids", *J. Non-Newtonian Fluid Mech.* **1991**, *40*, 155

8. H. Giesekus, "A Simple Constitutive Equation for Polymer Fluids Based on the Concept of Deformation-Dependent Tensional Mobility", *J. Non-Newtonian Fluid Mech.* **1982**, *11*, 69

9. R. B. Bird, R. C. Armstrong, O. Hassager, "Dynamics of Polymeric Liquids, Vol. I", 2nd ed., John Wiley & Sons Press: New York, **1987**

10. E. S. G. Shaqfeh, S. J. Muller, R. G. Larson, "The effects of gap width and dilute solution properties on the viscoelastic Taylor-Couette instability", *J. Fluid. Mech.* **1992**, *235*, 285

11. N. Phan-Thien, "Cone-and-plate flow of the Oldroyd-B fluid is unstable", *J. Non-Newtonian Fluid Mech.* **1985**, *17*, 37

12. S. J. Muller, R. G. Larson, E. S. G. Shaqfeh, "A purely elastic transition in Taylor-Couette flow", *Rheol. Acta* **1989**, *28*, 449

13. M. G. Hansen and F. Nazem, "Transient Normal Force Transducer Response in a Modified Weiddenberg Rheogoniometer", *Transaction of the Society of Rheology* **1975**, *19*, 21

14. C. S. Lee, Ph.D. Dissertation, University of Utah, Salt Lake City, **1995**

15. D. V. Boger, "A Highly Elastic Constant-Viscosity Fluid", *J. Non-Newtonian Fluid Mech.* **1977**, *3*, 87

16. B. H. Zimm, "Dynamics of Polymer Molecules in Dilute Solution: Viscoelasticity, Flow Birefringence and Dielectric Loss", *J. Chem. Phys.* **1956**, *24*, 269

17. Y. Hiki, T. Kosugi, "Relaxations in Polystyrene below the Glass Transition Studied by Internal Friction Measurement", *J. Non-Crystalline Solids* **2005**, *35*, 1300

18. J. Klein, "Evidence for reptation in an entangled polymer melt", *Nature* **1978**, *271*, 143

19. R. W. Whorlow, "Rheological Techniques", 2nd Edition, Ellis Horwood Limited Press: **1992**

20. T. N. G. Abbott, G. W. Bowen, K. Walters, "Some suggestions for new Rheometer Designs", Department of applied mathematics, University college of Wales, Penglais, Aberystwyth, **1970**

21. M. J. Miller, "The Complete Stress State of Five Viscoelastic Fluid in Viscometric Flow" Ph.D. Dissertation, University of Utah, Salt Lake City, **1994**

22. Seong-Gi Baek, "Novel rheological techniques applied to investigate rheology of liquid crystal polymers", Ph.D. Dissertation, University of Utah, Salt Lake City, **1991**

23. J. Z. Lou, "Rheological Study of a Polyisobutylene Boger Fluid Using Rod Climbing Rheometry" MS Thesis, University of Utah, Salt Lake City, **1992**

24. J.-Y. Lee, J. J. Magda, H. Hu, R. G. Larson, "Cone Angle Effect, Radial Pressure Profile, and Second Normal Stress Difference for Shear-thickening Wormlike Micelles", *J. Rheol.* **2002**, *46*, 195

25. Myoungbae Lee, Master of Science Thesis, Univeristy of Utah, Salt Lake City, **2004**

26. M. Lee, W. Huang, J.-W. Kim, J. J. Magda, S.-G. Baek, "Simultaneous Measurement of N_1 and N_2 for a Room Temperature PDMS Melt Using a Standard Torsional Rheometer Adapted with a Monolithic Pressure Sensor Plate, Congress Secretariat of the XIVth International Congress on Rheology - the Korean Society of Rheology - ICR2004, submitted

27. R. I. Tanner, "Engineering Rheology (Revised edition)", Clarendon Press: Oxford, New York, **1985**

28. K. Walters, “Rheometry”, Halsted Press: New York, **1975**

29. “Instruction Manual for R17 Weissenberg Rheogoniometer”, Sangamo Controls, Ltd.; Sussex, Great Britain

30. H. W. Greensmith, R. S. Rivlin, *Phil. Trans. Roy. Soc. A* **1953**, *245*, 399

31. G. Taylor, P. G. Saffman, *J. Aeron. Sci.* **1957**, *24*, 553

32. N. Adams, A. S. Lodge, “Rheological Properties of Concentrated polymer Solutions II. A Cone-and-plate and Parallel-plate pressure Distribution Apparatus for Determining Normal Stress Differences in Steady Shear Flow”, *Phil. Trans. Roy. Soc. A* **1964**, *256*, 149

33. D. J. Dudgeon, L. E. Wedgewood, “Flow in the Misaligned Cone-and-plate Rheometer”, *J. of Non-Newtonian Fluid Mech.* **1993**, *48*, 21

34. Ko Higashitani, A. S. Lodge, “Hole Pressure Error Measurements in Pressure-Generated Shear Flow”, *J. of Non-Newtonian Fluid Mech.* **1975**, *19*, 307

35. B. Bernstein, E. A. Kearsley, L. J. Zapas, “A Study of Stress Relaxation with Finite Strain”, *Journal of Rheology* **1963**, *7*, 391

36. A. S. Lodge, “Stress Relaxation after a Sudden Shear Strain”, *Rheol. Acta* **1975**, *14*, 664

37. J. M. Niemiec, J. J. Pesce, G. B. McKenna, S. Skocypec, R. F. Garritano, “Anomalies in the Normal Force Measurement when Using a Force Rebalance Transducer”, *J. Rheol.* **1996**, 323

38. J. Meissner, “Modification of the Weissenberg Rheogoniometer for Measurement of Transient Rheological Properties of Molton Polyethylene undershear. Comparison with Tensile Data”, *J. Applied Polymer Sci.* **1972**, *16*, 2877

39. Ramachandran and E. R. Christiansen, “Reduction of Axial Compliance in an R-17 Weissenberg Rheogoniometer”, *Journal of Rheology* **1980**, *24*, 32531. 2

40. M. Gottlieb, C. W. Macosko, “The Effect of Instrument Compliance on Dynamic Rheological Measurement”, *Rheol. Acta* **1982**, *21*, 90

41. L. J. Zapas and G. B. McKenna, “An Analysis of the Corrections to the Normal Force Response for the Cone-and-Plate Geometry in Single-Step Stress Relaxation Experiments”, *Journal of Rheology* **1989**, *33*, 69

42. C. M. Vrentas, W. W. Graessley, "Relaxation of Shear and Normal Stress Components in Step-stain Experiments", *J. Non-Newtonian Fluid Mech.* **1981**, *9*, 339

43. E. E. Ambrosius, R. D Fellows, A. D. Brickman, "Mechanical Measurement and Instrumentation", the Ronald Press Company, New York, **1966**

44. Seong-Gi Baek, J. J. Magda, "Monolithic Rheometer Plate Fabricated Using Silicon Micromachining Technology and Containing Miniature Pressure Sensors for N_1 and N_2 Measurements", *J. Rheol.* **2003**, *47*, 1249

45. S. A. Hutcheson, X. F. Shi and G. B. McKenna, "Performance Comparison of a Custom Strain Gage Based Load Cell with a Rheometric Series Force Rebalance Transducer", *ANTEC*, **2004**, 2272

46. R. F. Ginn, A. B. Metaner, "Measurement of Stresses Developed in Steady Laminar Shearing Flows of Viscoelastic Media", *J. Rheol.* **1969**, *13*, 429

47. J. D. Huppler, E. Ashare, and L. A. Holmes, "Rheological properties of three solutions", *Trans. Soc. Rheol.* **1967**, *11*, 159-179

48. A. B. Metzner and J. L. White, "Measurement of Normal Stresses", *Trans. Soc. Rheol.* **1963**, *7*, 295

49. M. Keentok, A. G. Georgescu, A. A. Sherwood, and R. I. Tanner, "The Measurement of the Second Normal Stress Difference for Some Polymeric Solutions", *J. Non-Newtonian Fluid Mech.* **1980**, *6*, 303

50. Y. Kuo, R. I. Tanner, "On the Use of Open-channel Flows to Measure the Second Normal Stress Difference", *Rheol. Acta* **1974**, *13*, 443

51. J. P. Berry, J. Batchelor, "Measurement of the first and second normal stress differences: correlation of four experiments", *J. Fluid Mech.* **1968**, *44*, 419

52. J. Batchelor, J. P. Berry, F. Horsfall, "Die swell in elastic and viscous fluids", *Polymer* **1973**, *14*, 297

53. A. Kaye, A. S. Lodge, and D. G. Vale, "Determination of Normal Stress Differences in Steady Shear Flow. II: Flow Birefringence, Viscosity, and Normal Stress Data for a Polyisobutene Liquid", *Rheol. Acta* **1968**, *7*, 368

54. R. Jackson, A. Kaye, "The Measurement of the Normal Stress Differences in a Liquid Undergoing Simple Shear Flow Using a Cone and plate Total Thrust Apparatus only", *Brit. Appl. Phys.* **1966**, *17*, 1355

55. B. D. Marsh, JRA. Pearson, "The Measruement of Normal-stress Differences Using Cone-and-plate Total Thrust apparatus", *Rheol. Acta* **1968**, *4*, 464

56. N. Ohl, W. Gleissle, “The Second Normal Stress Difference for Pure and Highly Filled Viscoelastic Fluids”, *Rheol. Acta* **1992**, *31*, 294

57. E. F. Brown, W. R. Burghardt, H. Kahvand, D. C. Venerus, “Comparision of Optical and mechanical Measurements of Second Normal Stress Difference Relaxation Following Step Strain”, *Rheol. Acta* **1995**, *34*, 221

58. D. S. Malkus, W. G. Pritchard, M. Yao, “The Hole-pressure Effect and Viscometry”, *Rheol. Acta* **1992**, *31*, 521

59. E. A. Kearsley, “Measurement of Normal stress by Means of Hole Pressure”, *Trans. Soc. Rheol.* **1973**, *17*, 617

60. H. E. van Es, “A new method for determining the second normal stress difference in viscoelastic fluids”, *Rheol. Acta* **1974**, *13*, 905

61. J. Meissner, R. W. Carbella, J. Hostettler, “Measuring Normal Stress Differences in polymer Melt Shear Flow”, *J. Rheol.* **1989**, *33*, 843

62. H. Eggers, P. Schümmer, “A New Method for Determinnation of Normal-stress Differences in Highly Ciscoelastic Substances Using a ModifiedWeissenberg Rheometer”, *J. Rheol.* **1994**, *38*, 1169

63. Thomas Schweizer, “Measurement of the First and Second Normal stress Differnces in a Polystyrene Melt with a Cone and Partitional Plate Tool”, *Rheol. Acta* **2002**, *41*, 337

64. G. S. Ribeiro, M. S. Arney, J. Feng, D. D. Joseph, “Rod Climbing and Normal Stresses in Heavy Crude Oils at Low Shears”, *J. Rheol.* **1994**, *38*, 1251

65. L. D. Landro, M. Levi, D. Nichetti, A. Consolo, “Experimetal Determination of Rheological Properties of Poly(dimethylsiloxane)”, *European Polymer Journal* **2003**, *39*, 1831

66. B. E. Christiansen, W. R. Leppard, “Steady-state and osillatory Flow Properties of Polymer Solutions”, *Trans Soc Rheol.* **1974**, *18*, 1005

67. M. J. Miller, E. B. Christiansen, “The Stress State of Elastic Fluids in Viscometric Flow”, *AIChE J* **1972**, *18*, 600

68. J. J. Magda, S. G. Baek, K. L. DeVries, R. G. Larson, “Shear Flows of Liquid Crystalline Polymers: Measurements of the Second Normal Stress Difference and Doi Molecular Theory”, *Macromolecules* **1991**, *24*, 4460

69. J. J. Magda, C. S. Lee, S. J. Muller, R. G. Larson, “Rheology, Flow Instabilities, and Shear-induced Diffusion in Polystyrene Solutions”, *Macromolecules* **1994**, *26*, 1187

70. J. J. Magda, S. G. Baek, "Concentrated Entangled and Semidilute Entangled polystyrene Soltuions and the Second Normal Stress Difference", *polymer* **1994**, *35*, 1187

71. G. Brindley and J. M. Broadbent, "The measurements of normal stress differences in a cone-and-plate rheogoniometer using flush-mounted pressure transducers", *Rheol. acta* 1973, *12*, 48

72. R. I. Tanner and M. Keentok, "Shear Fracture in Cone-Plate Rheometry", *J. Rheol.* **1983**, *27*, 47

73. M. Keentok, S.-C. Xue, "Edge Fracture in Cone-plate and Parallel Plate Flows", *Rheol. acta* **1999**, *38*, 321

74. M. T. Ghannam, M. N. Esmail, "Rheological Properties of poly(methylsiloxane)", *Ind. Eng. Chem. Res.* **1998**, *37*, 1335

75. P. B. Leezenberg, M. D. Fayer, C. W. Frankl, "Photophysical studies of probes bound to cross-link junctions in poly(dimethy1 siloxane) elastomers and nanocomposites", *Pure & Appl. Chem.* **1996**, *68*, 1381

76. H. Allcock, F. Lampe, *Contemporary Polymer Chemistry*; Prentice-Hall Inc. Press: Englewood Cliffs, NJ, **1981**

77. http://www.fitzchem.com/mfg_rhodia.html

78. J. C. Lotters, W. Olthuis, P. H. Veltink, P. Bergveld, "The mechanical properties of the rubber elastic polymer polydimethylsiloxane for sensor applications", *J Micromech Microeng* **1997**, *7*, 145

79. J. C. McDonald, D. C. Duffy, J. R. Anderson, D. T. Chiu, H. Wu, O. J. A. Schueller, G. M. Whitesides, "Fabrication of microfluidic systems in poly(dimethylsiloxane)", *Electrophoresis* **2000**, *21*, 27

80. H. Hillborg, J. F. Ankner, U. W. Gedde, G. D. Smith, H. K. Yasuda, K. Wikstrom, "Crosslinked polydimethylsiloxane exposed to oxygen plasma studied by neutron reflectometry and other surface specific techniques", *Polymer* **2000**, *41*, 6851

81. J. N. Lee, C. Park, G. M. Whitesides,, "Solvent Compatibility of Poly(dimethylsiloxane)-Based Microfluidic Devices", *Anal. Chem.* **2003**, *75*, 6544

82. http://polymers.msel.nist.gov/

83. M. Elwenspoek and H. Jansen, "Silicon Micromachining", Cambridge University Press: **1998**